

Supporting Information

Design of TNFR Peptide Agonists for Inducing Receptors Oligomerization and Cell Apoptosis

Yixuan Liu,^{a, b} and Hao Wang,^{a, b*}

^aCAS Key Laboratory for Biomedical Effects of Nanomaterials and Nanosafety, CAS Center for Excellence in Nanoscience, National Center for Nanoscience and Technology (NCNST), Beijing, 100190, China.

^bCenter of Materials Science and Optoelectronics Engineering, University of Chinese Academy of Sciences, Beijing 100049, China.

*wanghao@nanoctr.cn

Table of contents

1 MATERIAL AND METHODS	4
2 PEPTIDE DESIGN	4
2.1 β -Sheet Scaffold Identification	4
2.2 AlphaFold3 Predictions	4
2.3 Structural Analysis and Homology Modeling.....	7
2.4 Molecular Docking	8
2.5 Molecular Dynamics Simulations	10
2.5.1 System Preparation and Simulation Parameters	16
2.5.2 System Configuration and Initialization	16
2.5.3 Simulation Protocol and Equilibration	17
2.5.4 Production Simulations and Analysis	17
3 CHEMICAL SYNTHESIS PROCEDURE	17
3.1 Peptide Synthesis.....	17
3.2 Preparation and Characterization of Cy5-labeled Peptides	21
4 BIOPHYSICAL CHARACTERIZATION AND INTERACTION ANALYSIS	26
4.1 Bio-Layer Interferometry (BLI) Affinity Test	26
4.2 Circular Dichroism (CD) Spectroscopy	28
4.3 Immunoprecipitation and Size Exclusion Chromatography	31
5 CELL VIABILITY ASSAY	31
5.1 General Information	31
5.2 CTG Assay of AP, W10, EIA and EPR	31
6 CONFOCAL MICROSCOPY	36
6.1 Plasmid Construction and Transfection	36

6.2 Confocal Microscopy for colocalization and NF- κ B translocation	36
6.3 Nuclear Localization of CD95	36
6.4 NF- κ B Activation and Apoptotic Signaling	39
One-way ANOVA analysis of NF- κ B nuclear translocation in peptide-treated NF- κ B-GFPspark HeLa cells	44
7 APOPTOSIS ASSAY AND IMMUNOBLOTTING	44
7.1 Apoptosis Assay	44
7.2 Immunoblotting	45

1 Material and Methods

Recombinant human CD95/Fas extracellular domain (#10217-H08H, 100 µg) and recombinant human DR5/TRAIL-R2 extracellular domain (#10465-H49H-B, 20 µg) were purchased from Sino Biological (Beijing, China). Hoechst 33342 was obtained from Life Technologies (Carlsbad, USA). Lipofectamine 2000 and Opti-MEM were purchased from Invitrogen (Carlsbad, USA). CellTiter-Glo Luminescent Cell Viability Assay kit was obtained from Promega (Madison, USA). CD95-GFPSpark (#HG10217-ACG), DR5-GFPSpark (#HG10465-ACG), and NF-κB-GFPSpark (#HG12054-ANG) plasmids were purchased from Sino Biological (Beijing, China). Immunoprecipitation kit with Protein G magnetic beads (#P2177S) was obtained from Beyotime (Shanghai, China). Anti-CD95 monoclonal antibody (**APO-1**, #ab133619) was purchased from Abcam (Cambridge, UK). Cy5-NHS ester (≥90%, #146368-14-1) was obtained from ACMEC (Shanghai, China). Fmoc-protected amino acids and resins for peptide synthesis were purchased from GL Biochem (Shanghai, China). DMEM and RPMI-1640 cell culture media, fetal bovine serum (FBS), penicillin, and streptomycin were obtained from Gibco (Waltham, USA). HT29, COLO205, MDA-MB-231, and HEK293 cell lines were purchased from ATCC (Manassas, USA). All cells were maintained at 37°C in a humidified atmosphere with 5% CO₂. All reagents were of analytical grade and used as received. Water used in all experiments was purified using a Milli-Q system.

2 Peptide Design

2.1 β-Sheet Scaffold Identification

The crystal structure of death receptor 5 (DR5)-tumor related apoptosis inducing ligand (TRAIL) complex (PDB: 1D4V) was analyzed using PyMOL (v2.5.0, Schrödinger, LLC). Interaction interfaces were identified through distance-based analysis (cutoff 4.5 Å) to locate key interacting residues.

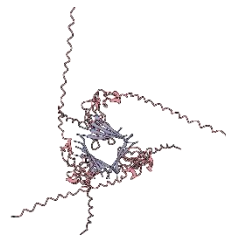
2.2 AlphaFold3 Predictions

Peptide-receptor complex structures were generated using the AlphaFold3 online server (<https://alphafoldserver.com/>). For each sequence, five models were generated, and the highest-confidence model (ranked by pLDDT score) was selected for further analysis. Predictions were performed using the standard parameters provided by the online server, with 'monomer' mode selected for 1:1 interactions and 'multimer' mode for oligomeric complexes.

Among all peptides, only YYIYSQTYFRFQ (**D5Y**) formed highly symmetrical nanoclusters when complexed with three DR5 receptors as predicted by AlphaFold3, while other peptides exhibited irregular or asymmetrical nanocluster structures. We implemented a quantitative scoring system in PyMOL that evaluates nanocluster formation ability using four key metrics: symmetry (uniformity of distances to geometric center), regularity (consistency of inter-chain distances), planarity (degree of two-dimensional arrangement as determined by principal component analysis), and radial distribution (angular uniformity in three-dimensional space). These metrics were combined into a comprehensive nanocluster score with weights of 0.35, 0.35, 0.15, and 0.15, respectively. Through this systematic assessment, **D5Y** achieved the highest score (0.79), confirming its superior ability to form well-ordered nanoclusters. We postulate that this regular nanocluster arrangement facilitates optimal receptor proximity and orientation for subsequent DR5 oligomerization and signaling. The detailed scores for all peptides are shown in **Table S1**. The corresponding AlphaFold3 predicted structures are presented in Figure S1-S2.

Table S1. Nanocluster formation score analysis of peptides complexed with DR5

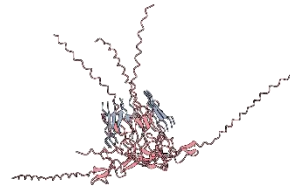
Sequence	symmetry	regularity	planarity	radial_distribution	nano_cluster_score
YYIYSQTYFRFQ	0.97	0.64	0.99	0.54	0.79
VCQCEEGT	0.85	0.73	0.77	0.66	0.77
TFREEDSPEMCRK	0.91	0.60	1.00	0.52	0.76
QTYRFRQ	0.88	0.62	0.97	0.54	0.75
IYSQTYRFRQ	0.93	0.56	0.99	0.51	0.75
TYRFRQ	0.85	0.64	0.93	0.56	0.74
SQTYRFRQ	0.90	0.58	1.00	0.52	0.74
YSQTYRFRQ	0.91	0.56	1.00	0.49	0.74
YIYSQTYRFRQ	0.88	0.59	0.93	0.53	0.73
TYFRFQE	0.94	0.53	0.93	0.45	0.72
TYFRFQEE	0.82	0.59	1.00	0.52	0.72
YFRFQ	0.79	0.62	1.00	0.52	0.72
VCQCEEGTFREED	0.85	0.51	0.93	0.45	0.68



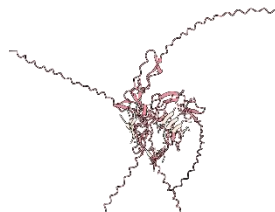
YIYSQTYRFRQ



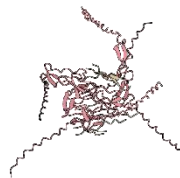
IYSQTYRFRQ



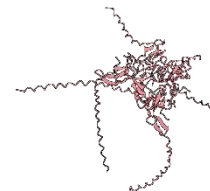
YSQTYRFRQ



SQTYRFRQ



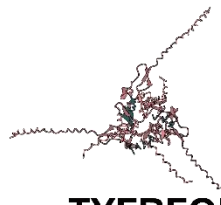
QTYRFRQ



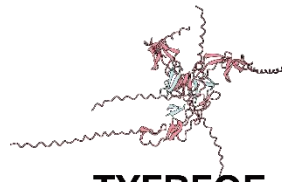
TYRFRQ



YFRFQ



TYFRFQEE



TYFRFQE

Figure S1. Complexes formed by TRAIL-derived peptides with DR5 under AlphaFold3 prediction conditions (stoichiometric ratio of peptide = 10:3).

TFREEDSPEMCRK VCQCEEGTFREED VCQCEEGT

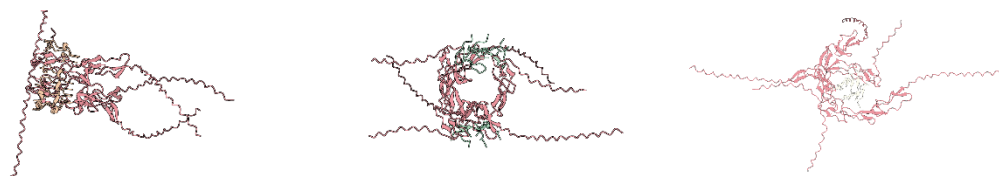


Figure S2. Complexes formed by DR5-derived peptides with DR5 under AlphaFold3 prediction conditions (stoichiometric ratio of peptide = 10:3).

2.3 Structural Analysis and Homology Modeling

The crystal structure of DR5-TRAIL complex (PDB: 1D4V) was analyzed using PyMOL (v2.5.0, Schrödinger, LLC). Interaction interfaces were identified through distance-based analysis (cutoff 4.5 Å) to locate key interacting residues. For CD95L, which lacks a crystal structure with CD95, sequence alignment with TRAIL was performed using Clustal Omega to identify homologous regions for scaffold design. Similarly, we utilized the scoring system mentioned above to evaluate **EIA**, **EPR**, **ERM**, **RIP**, **W10**, and **AP** as shown in **Table S2**. The AlphaFold3 predicted structures of **EIA**, **EPR**, **ERM**, **RIP** with three DR5 oligomers, and **W10** and **AP** with three CD95 oligomers are shown in Figure S3.

Table S2. Nanocluster formation score analysis of designed peptides complexed with DR5 and CD95

Peptide ID	symmetry	regularity	planarity	radial_distribution	nano_cluster_score
EIA	0.76	0.63	0.87	0.59	0.70
EPR	0.83	0.71	0.80	0.64	0.75
ERM	0.91	0.63	0.84	0.54	0.75
RIP	0.87	0.75	0.73	0.64	0.77
W10	0.65	0.56	0.97	0.51	0.64
AP	0.62	0.59	0.87	0.57	0.64

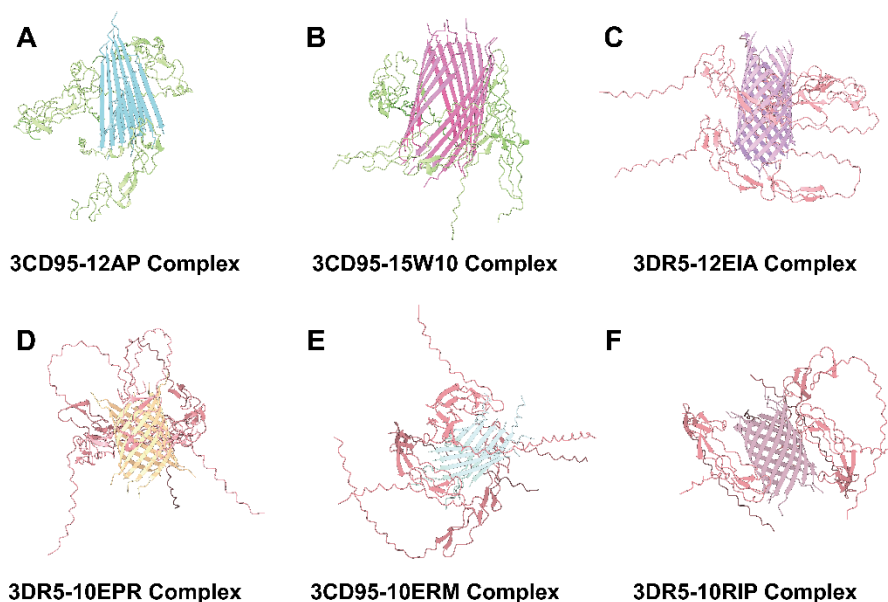


Figure S3. AlphaFold3 predicted structures of death receptor complexes with binding peptides. Computational models showing the predicted molecular interactions between (A) CD95 and peptide **AP**, (B) CD95 and peptide **W10**, (C) DR5 and peptide **EIA**, (D) DR5 and peptide **EPR**, (E) DR5 and peptide **ERMPCVEQYYIYSQTYFRFQ (ERM)**, and (F) DR5 and peptide **RIPCVRLEYIYSQTYFRFQ (RIP)**. The structures highlight key binding interfaces that may mediate receptor-peptide interactions. These models provide structural insights into the molecular basis of death receptor recognition by various peptide ligands.

2.4 Molecular Docking

The structures of selected complexes (**D5Y**, **EIA**, **EPR** with DR5, and **W10**, **AP** with CD95) in 1:1 ratio were first predicted using AlphaFold3 as shown in Figure S4. Following structure prediction, binding affinities between all peptides and their respective receptors were assessed using GNINA (v1.0) with the default scoring function. Receptor structures were prepared using AutoDockTools, and ligand structures were prepared using OpenBabel. Docking was performed with exhaustiveness=32 and a search space encompassing the expected binding site based on the original ligand position.

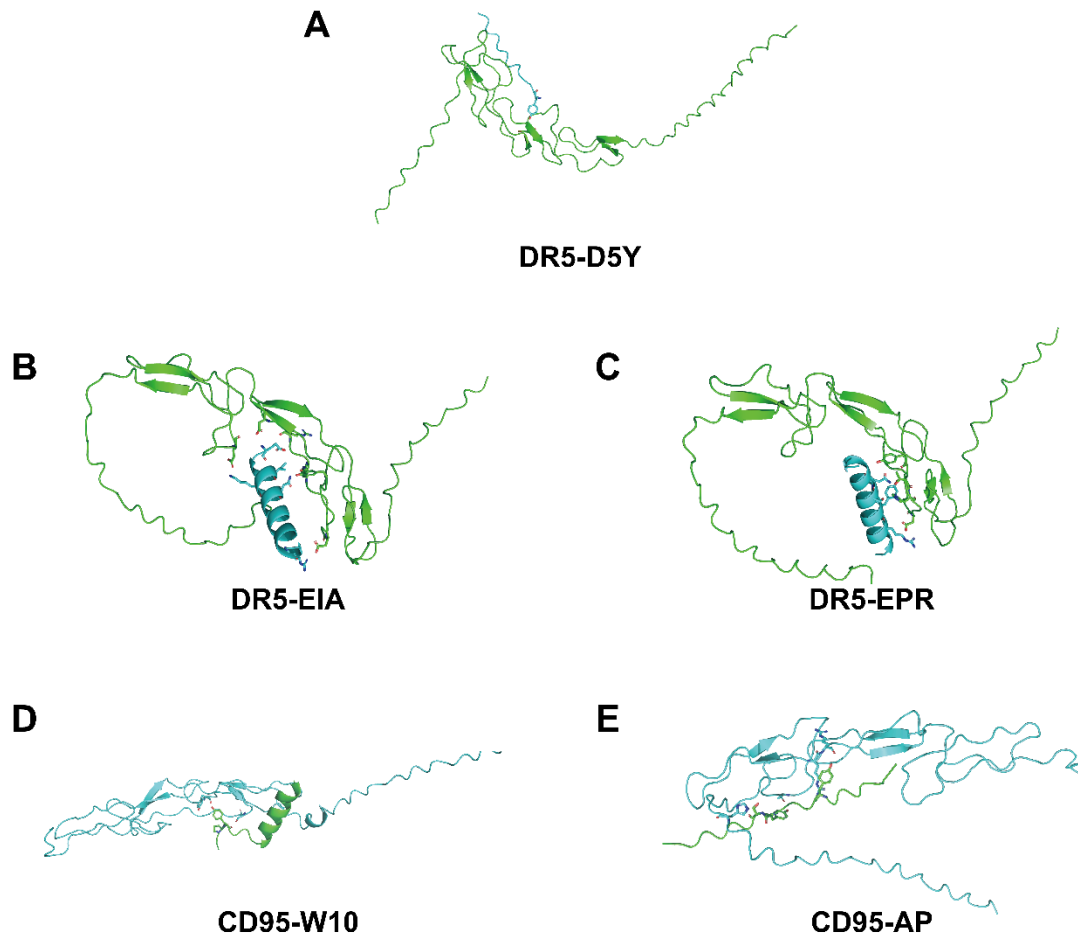


Figure S4. AlphaFold3-predicted structures between death receptors and synthetic peptides. Left panels (A-E): Overall AlphaFold3-predicted structures with death receptors (green) and peptides (cyan). (A) DR5(green)-**D5Y**(cyan). (B) DR5(green)-**EIA** (cyan). (C) DR5(green)-**EPR** (cyan). (D) CD95(cyan)-**W10**(green). (E) CD95(cyan)-**AP** (green).

Hydrogen bonding patterns between peptides and receptors were analyzed using the polar contacts function in PyMOL (v2.5.0, Schrödinger, LLC) with a distance cutoff of 3.5 Å and an angle cutoff of 30°. Polar contacts were specifically examined between peptide and receptor chains to systematically identify the number and position of hydrogen bonds. Each hydrogen bond was characterized by donor and acceptor atoms, bond distance, and bond angle to ensure accurate representation of the intermolecular interactions. This systematic analysis revealed distinct patterns of hydrogen bonding that correlated with the observed binding affinities, with more extensive hydrogen bonding networks corresponding to higher binding affinities in the optimized peptides compared to the original D5Y scaffold.

The docking calculations were performed on a high-performance computing cluster with 16 cores and 32 GB RAM. For each peptide-receptor pair, 100 independent docking runs were conducted to ensure thorough sampling of potential binding modes. The binding free energies were calculated using the built-in scoring function, and the lowest energy conformations were selected for further analysis. The raw data from GNINA molecular docking for all peptides is presented in **Table S3**.

Table S3. GNINA molecular docking results including binding affinities, CNN scores and CNN affinity.

Peptide ID	affinity (kcal/mol)	CNN pose score	CNN affinity
D5Y	-5.24	0.23	7.33
EIA	-5.10	0.29	9.42
EPR	-4.83	0.32	9.88
ERM	-4.27	0.34	8.51
RIP	-2.56	0.21	8.89
AP	-5.86	0.50	8.43
W10	-4.58	0.23	9.41

2.5 Molecular Dynamics Simulations

GROMACS (v2022.2) was used for all molecular dynamics simulations. Peptide-receptor complexes were solvated in a cubic box with TIP3P water and 0.15 M NaCl. Energy minimization was performed using the steepest descent algorithm until the maximum force was below 1000 kJ/mol/nm. NVT equilibration (100 ps, 300 K) was followed by NPT equilibration (100 ps, 300 K, 1 bar) using the Berendsen thermostat and barostat. Production runs (10 ns) were performed using the amber99sb-ildn force field with a 2 fs time step. Coordinates were saved every 100 ps for analysis. For each complex, three independent simulations were performed with different initial velocities. RMSD and RMSF analyses were performed using GROMACS analysis tools.

To investigate the stability of oligomeric complexes formed by peptides **W10** and **AP** with CD95, and peptides **EIA** and **EPR** with DR5 as predicted by AlphaFold3, we performed GROMACS molecular dynamics simulations over 10 ns, with triplicate runs for each complex. **Figure S5** illustrates the superimposed structures extracted at 0, 2, 4, 6, 8, and 10 ns for each peptide-receptor complex.

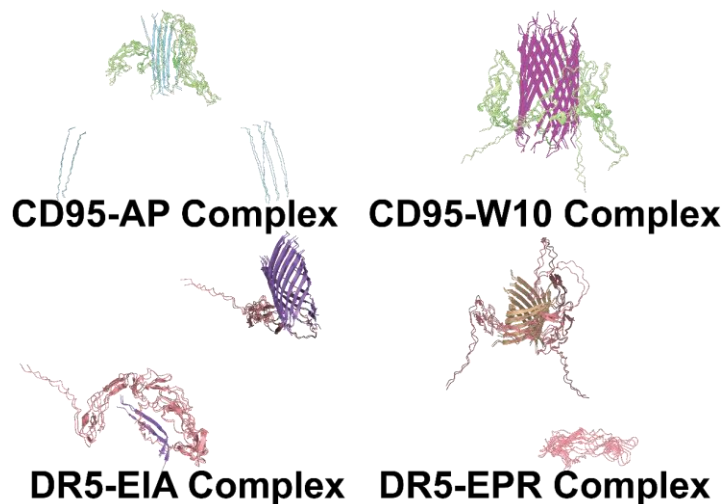


Figure S5. Molecular dynamics simulation visualizations of peptide-receptor complexes showing superimposed structures at different timepoints.

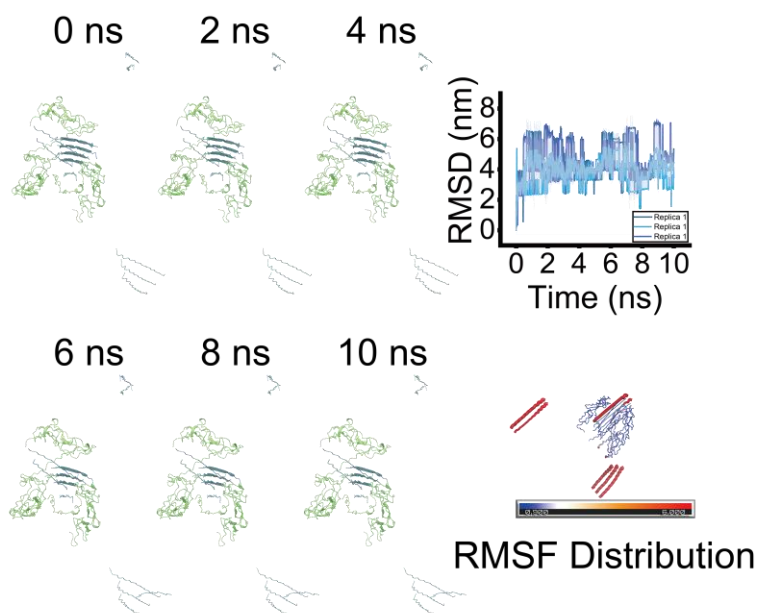


Figure S6. Average values from three replicates at 10 ns with RMSD values and RMSF mapping for CD95-AP complex.

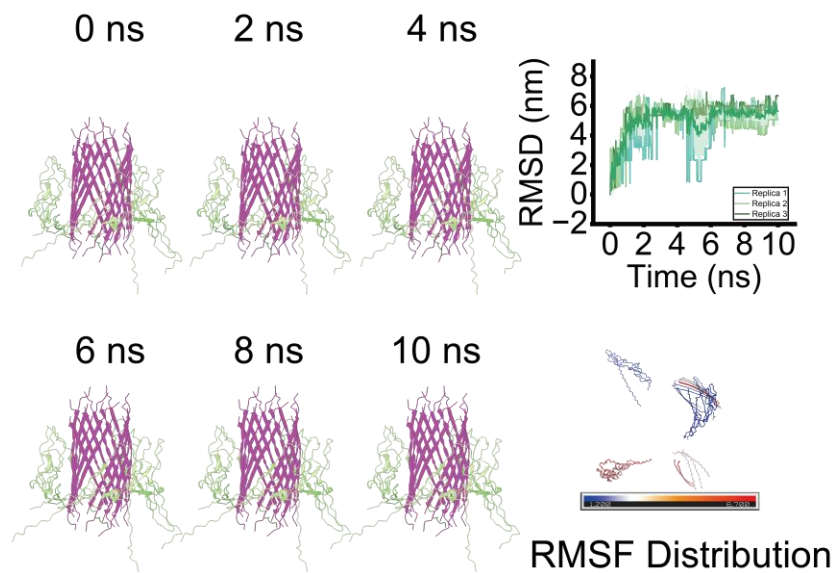


Figure S7. Average values from three replicates at 10 ns with RMSD values and RMSF mapping for CD95-W10 complex.

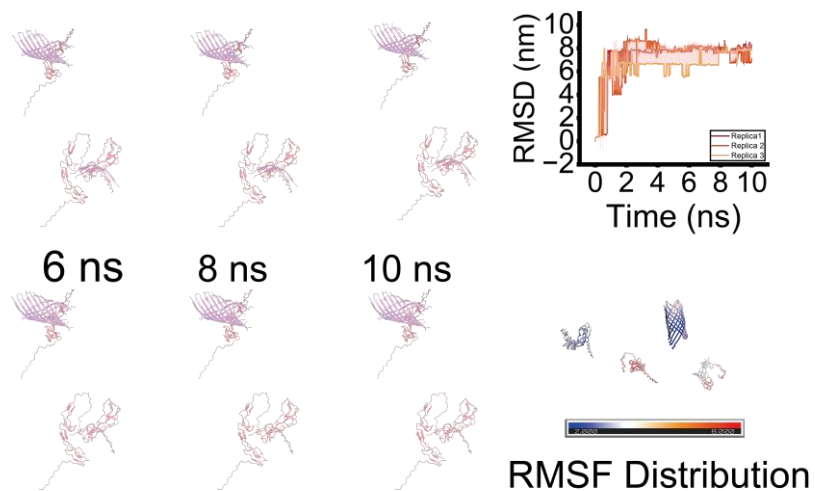


Figure S8. Average values from three replicates at 10 ns with RMSD values and RMSF mapping for DR5-EIA complex.

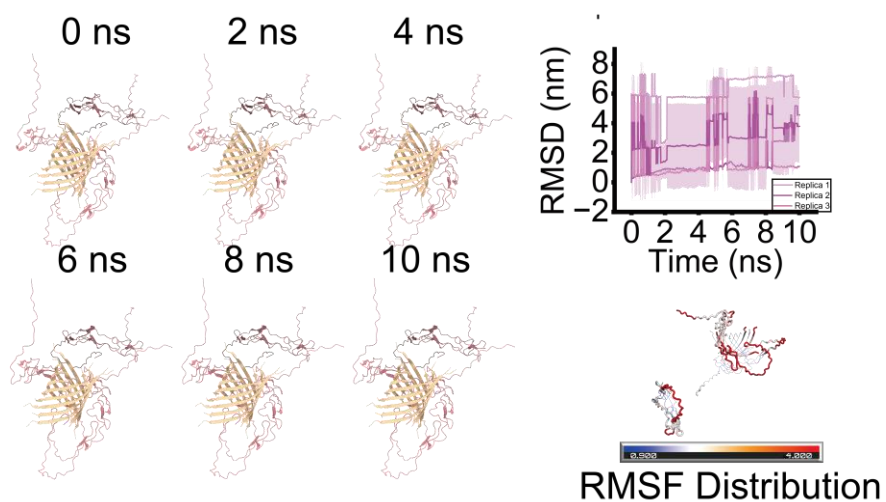


Figure S9. Average values from three replicates at 10 ns with RMSD values and RMSF mapping for DR5-EPR complex.

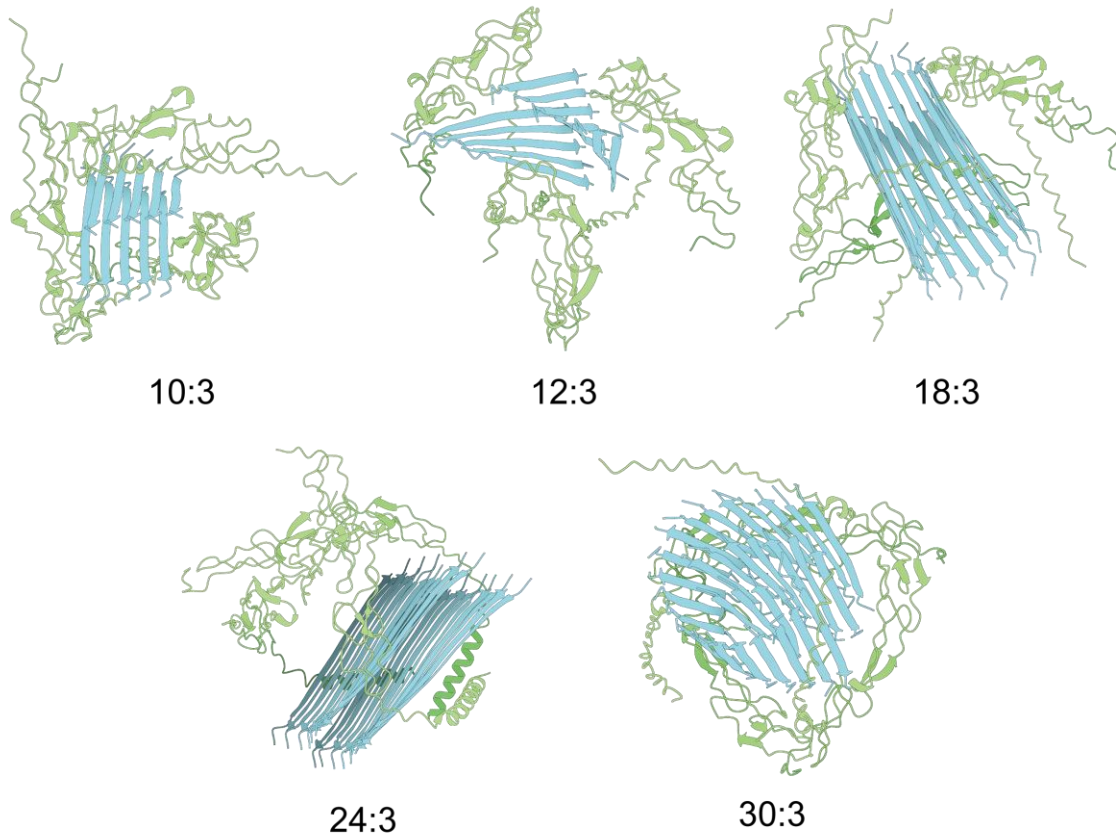


Figure S10. AlphaFold3-predicted structures of **AP** peptide-CD95 complexes at different stoichiometric ratios. Structural predictions showing the effect of varying peptide: receptor ratios on complex formation and stability. The stoichiometric ratios tested include 10:3, 12:3, 18:3, 24:3, and 30:3 (**AP**: CD95). CD95 receptors are shown in bright green, and **AP** peptides are depicted in light blue.

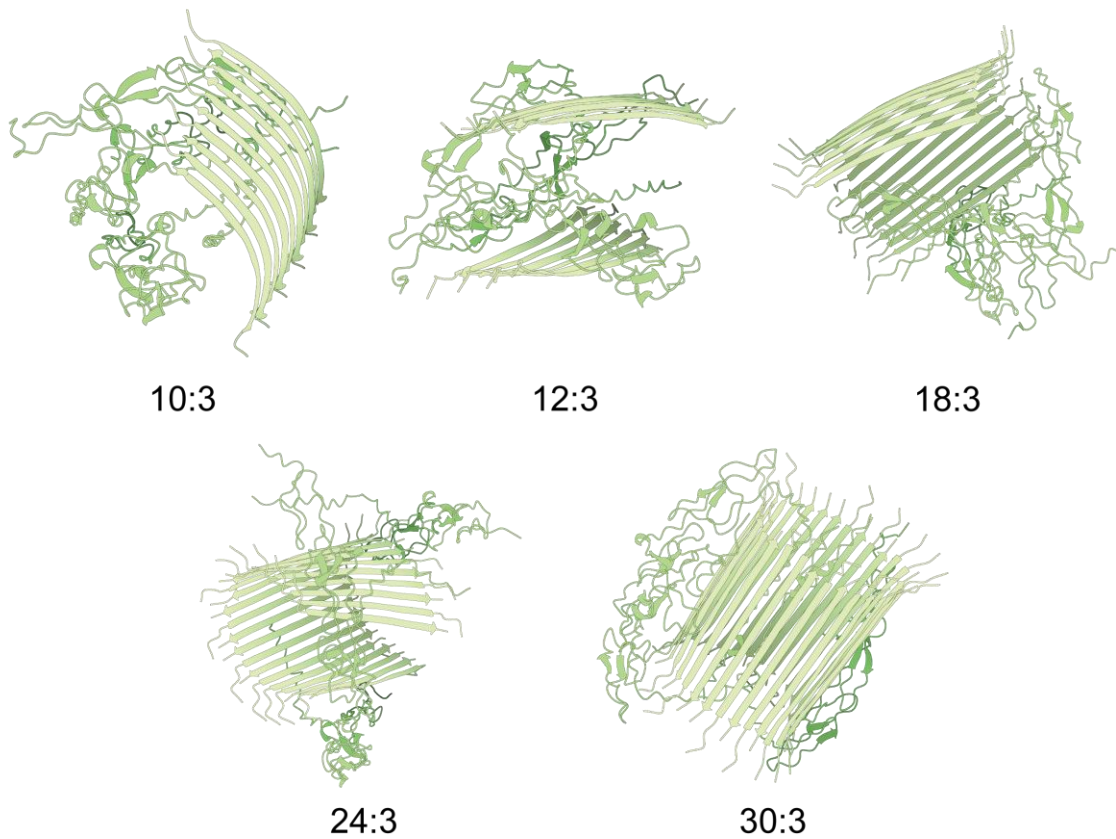


Figure S11. AlphaFold3-predicted structures of **W10** peptide-CD95 complexes at different stoichiometric ratios. Structural predictions showing the effect of varying peptide: receptor ratios on complex formation and stability. The stoichiometric ratios tested include 10:3, 12:3, 18:3, 24:3, and 30:3 (**W10**: CD95). CD95 receptors are shown in bright green, and **W10** peptides are depicted in light green.

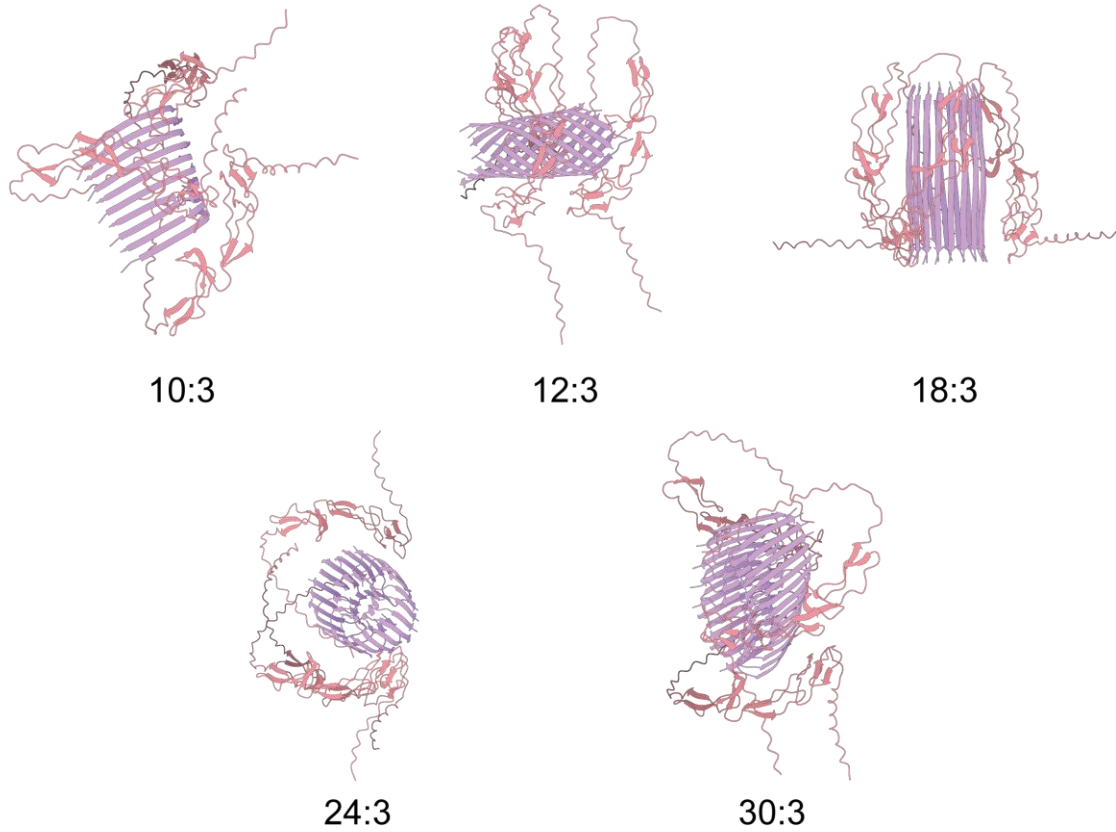


Figure S12. AlphaFold3-predicted structures of **EIA** peptide-DR5 complexes at different stoichiometric ratios. Structural predictions showing the effect of varying peptide: receptor ratios on complex formation and stability. The stoichiometric ratios tested include 10:3, 12:3, 18:3, 24:3, and 30:3 (**EIA**: DR5). DR5 receptors are shown in pink, and **EIA** peptides are depicted in purple.

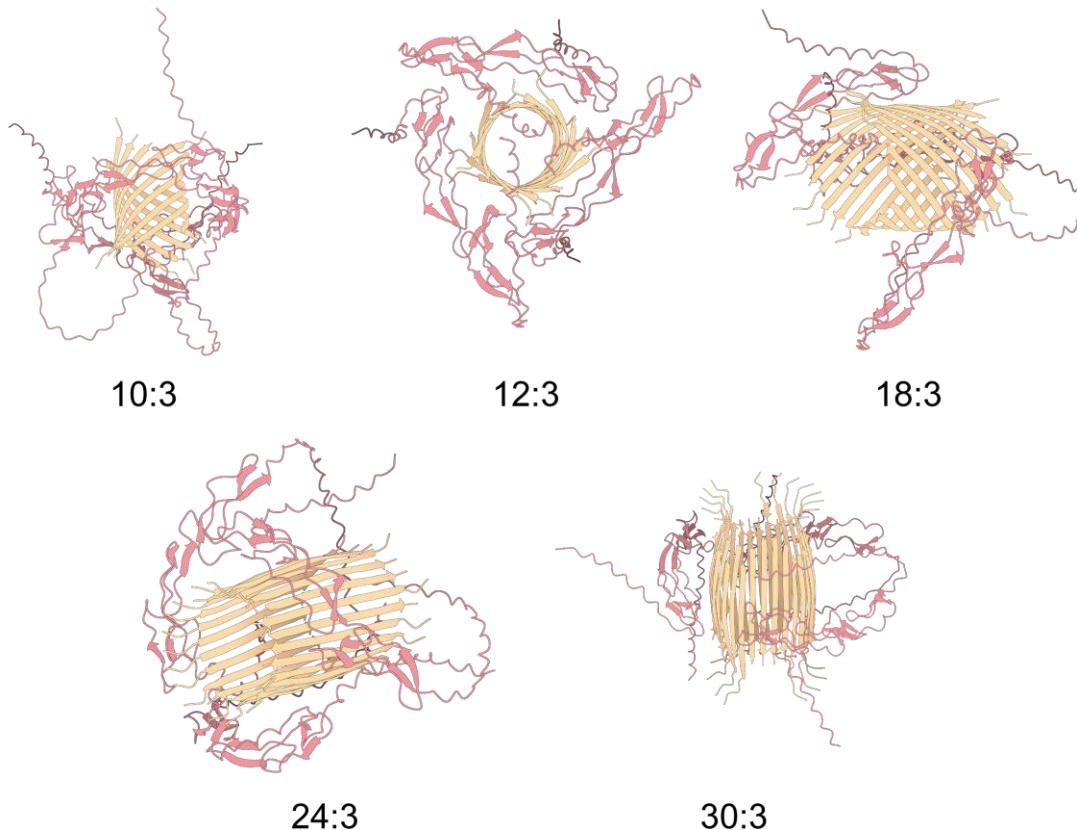


Figure S13. AlphaFold3-predicted structures of EPR peptide-DR5 complexes at different stoichiometric ratios. Structural predictions showing the effect of varying peptide: receptor ratios on complex formation and stability. The stoichiometric ratios tested include 10:3, 12:3, 18:3, 24:3, and 30:3 (EPR peptide:DR5). DR5 receptors are shown in pink, and EPR peptides are depicted in light orange.

2.5.1 System Preparation and Simulation Parameters

GROMACS (v2022.2) was used for all molecular dynamics simulations. Peptide-receptor complexes were solvated in a cubic box with TIP3P water and 0.15 M NaCl. Energy minimization was performed using the steepest descent algorithm until the maximum force was below 1000 kJ/mol/nm. NVT equilibration (100 ps, 300 K) was followed by NPT equilibration (100 ps, 300 K, 1 bar) using the Berendsen thermostat and barostat. Production runs (10 ns) were performed using the amber99sb-ildn force field with a 2 fs time step. Coordinates were saved every 100 ps for analysis. For each complex, three independent simulations were performed with different initial velocities. RMSD and RMSF analyses were performed using GROMACS analysis tools.

2.5.2 System Configuration and Initialization

For each simulation, the peptide-receptor complex was centered in a dodecahedral box with a minimum distance of 1.0 nm from the complex to the box edge. The system was solvated using the SPC216 water model as implemented in GROMACS. Counter ions (Na⁺ and Cl⁻) were added both to neutralize the system and to achieve a physiological salt concentration of 0.15 M. The AMBER99SB-ILDN force field was selected due to its accurate representation of protein-peptide interactions and conformational dynamics. Each system contained approximately 70,000-85,000 atoms depending on the specific peptide-receptor complex.

2.5.3 Simulation Protocol and Equilibration

Prior to production simulations, each system underwent a rigorous preparation protocol: Energy minimization was conducted using the steepest descent algorithm with a maximum force tolerance of 1000 kJ/mol/nm to remove unfavorable steric clashes and optimize the geometry of the solvated complex. NVT equilibration was performed for 100 ps at 300 K using the V-rescale thermostat ($\tau_t = 0.1$ ps) with position restraints applied to all protein and peptide heavy atoms (restraint force constant = 1000 kJ/mol/nm²) to allow proper equilibration of the solvent around the complex. NPT equilibration followed for an additional 100 ps, maintaining temperature at 300 K with the V-rescale thermostat while introducing pressure coupling using the Berendsen barostat ($\tau_p = 2.0$ ps) to achieve a pressure of 1 bar. Position restraints were maintained during this phase.

2.5.4 Production Simulations and Analysis

Production molecular dynamics simulations were conducted for 10 ns with the position restraints removed. The leap-frog integrator was employed with a 2 fs time step, enabled by constraining hydrogen-containing bonds using the LINCS algorithm ($\text{lincs_order} = 4$, $\text{lincs_iter} = 1$). Long-range electrostatic interactions were treated using the Particle Mesh Ewald (PME) method with a real-space cutoff of 1.0 nm. Van der Waals interactions were truncated at 1.0 nm with a smoothing function applied. Temperature was maintained at 300 K using the V-rescale thermostat with separate coupling groups for protein and non-protein components ($\tau_t = 0.1$ ps). Pressure was controlled at 1 bar using the Parrinello-Rahman barostat ($\tau_p = 2.0$ ps) with isotropic coupling.

The stability and conformational dynamics of each peptide-receptor complex were evaluated through comprehensive RMSD and RMSF analyses. To ensure statistical validity, three independent replicate simulations were performed for each complex with different initial velocity distributions. Trajectory data was saved every 100 ps, generating 100 frames per simulation for subsequent analysis. This sampling frequency provided sufficient temporal resolution to capture relevant conformational transitions while maintaining manageable data volumes.

3 Chemical Synthesis Procedure

3.1 Peptide Synthesis

Peptides (**W10**, **AP**, **EIA**, and **EPR**) were synthesized using standard Fmoc solid-phase synthesis on a 2-chlorotrityl resin. The synthesis was performed on a 0.1 mmol scale. Fmoc deprotection was achieved using 20% piperidine in DMF (v/v) for 20 min. Amino acid coupling was performed using 10 equiv. of Fmoc-AA-OH, 10 equiv. of HBTU, and 10 equiv. of DIEA in DMF for 2 h. After synthesis, peptides were cleaved from the resin using TFA/TIS/H₂O (95:2.5:2.5, v/v/v) for 2 hours at room temperature. Crude peptides were purified by reversed-phase HPLC on a C18 column (Shimadzu Shim-pack GWS, 5 μ m, 4.6 \times 250 mm) using a 5-95% acetonitrile gradient containing 0.1% TFA at a flow rate of 1 mL/min. The identity and purity of each peptide were confirmed by analytical HPLC and high-resolution mass spectrometry (HRMS). For all peptides, the HPLC method was as follows: solvent A, 0.065% formic acid in 100% water; solvent B, 0.05% formic acid in 100% acetonitrile; 0 min-25 min, 5%-95% solvent B.

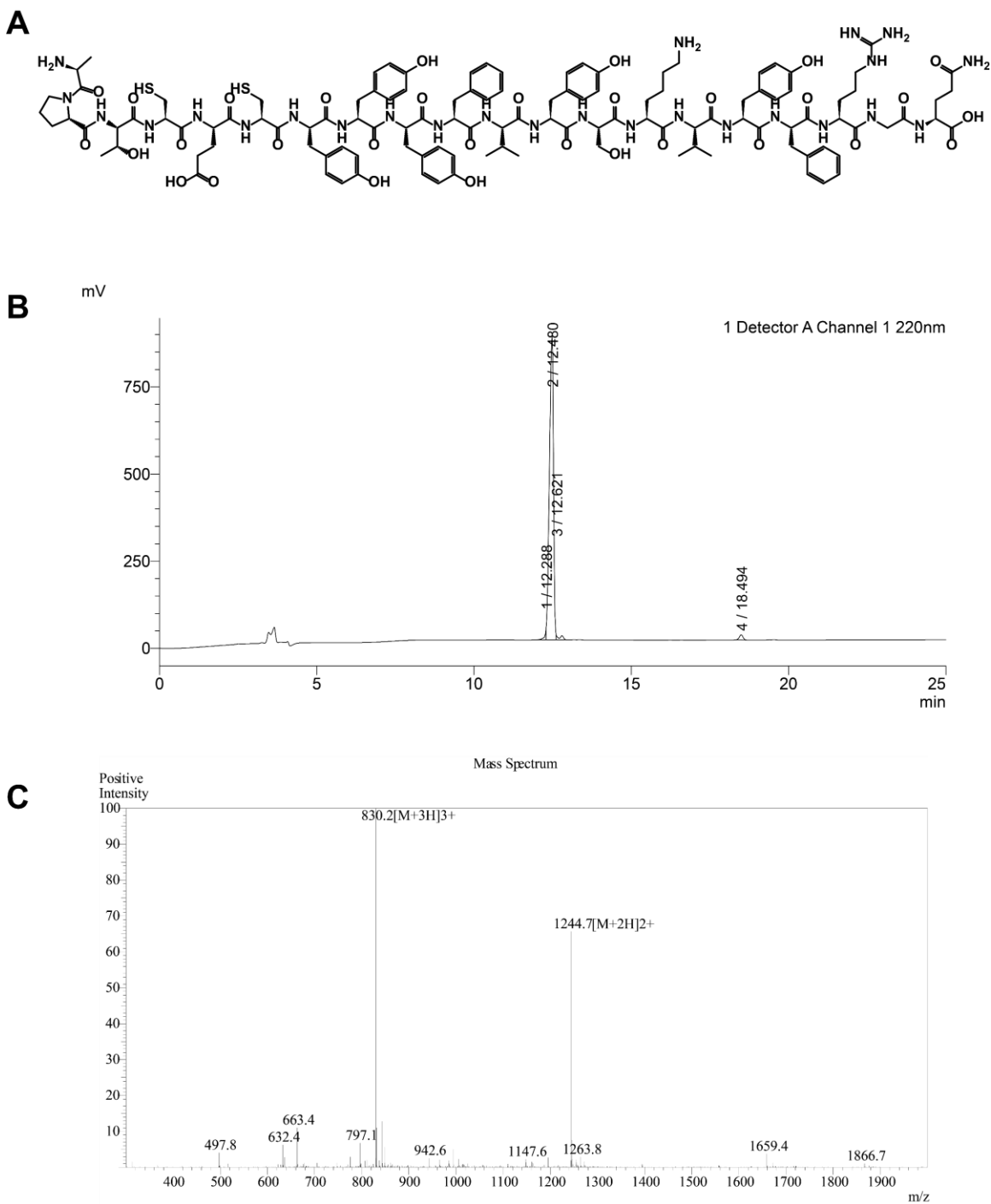


Figure S14. Characterization of AP. (A) Chemical structure of AP. (B) HPLC analysis of AP. (C) Mass spectrum analysis of AP.

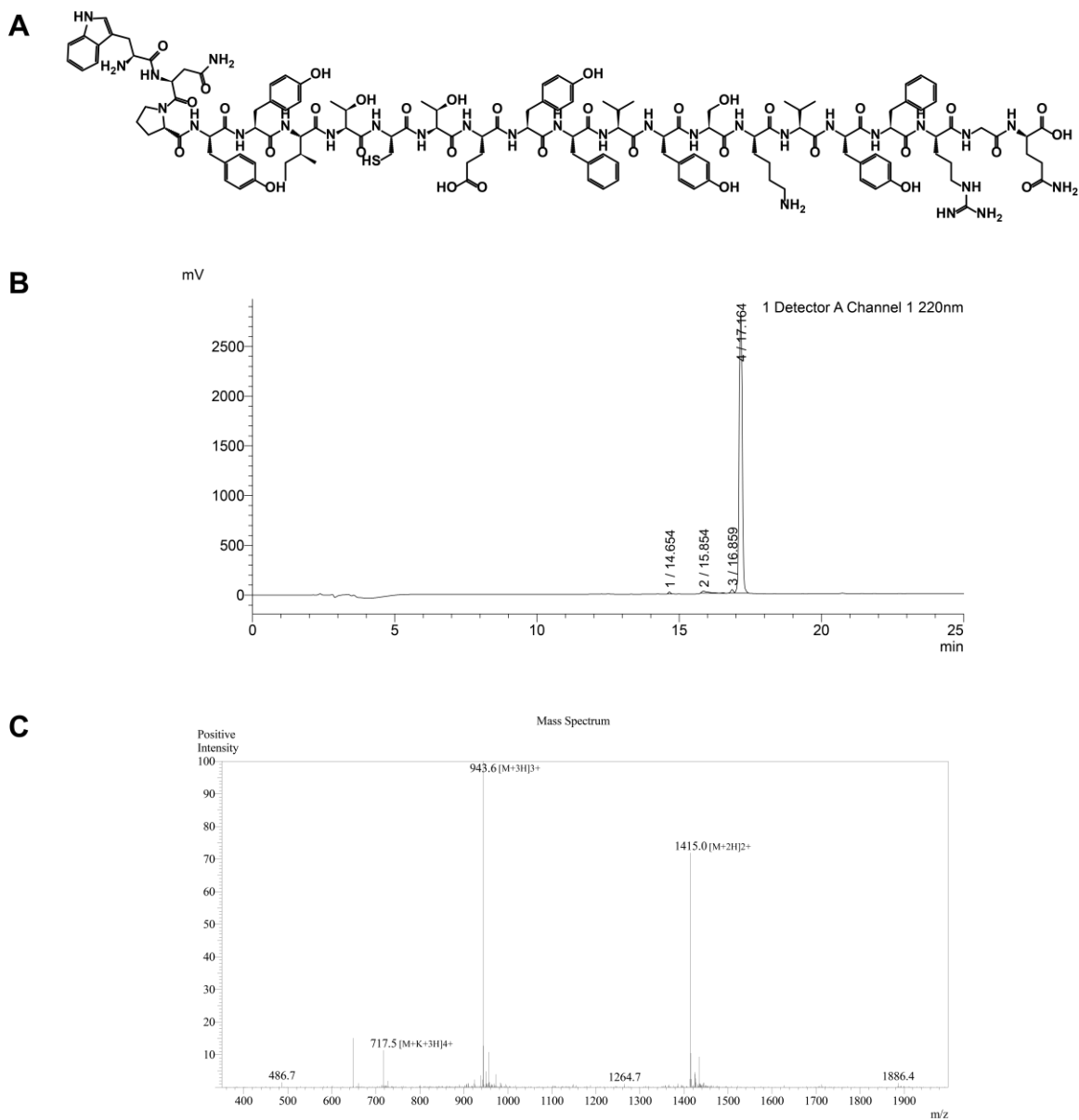


Figure S15. Characterization of **W10**. (A) Chemical structure of **W10**. (B) HPLC analysis of **W10**. (C) Mass spectrum analysis of **W10**.

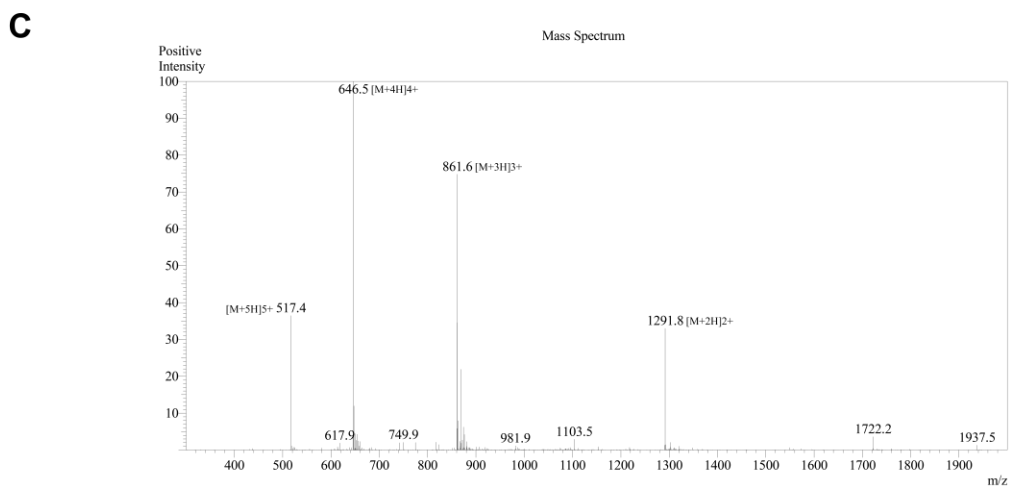
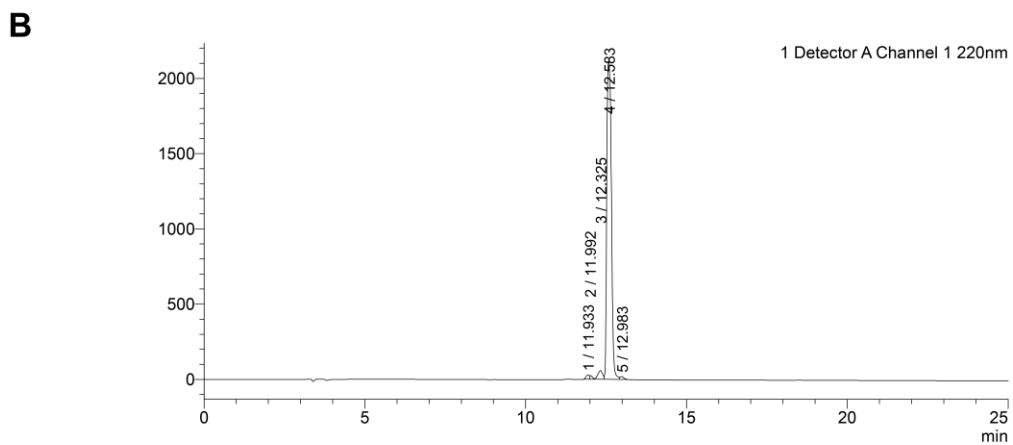
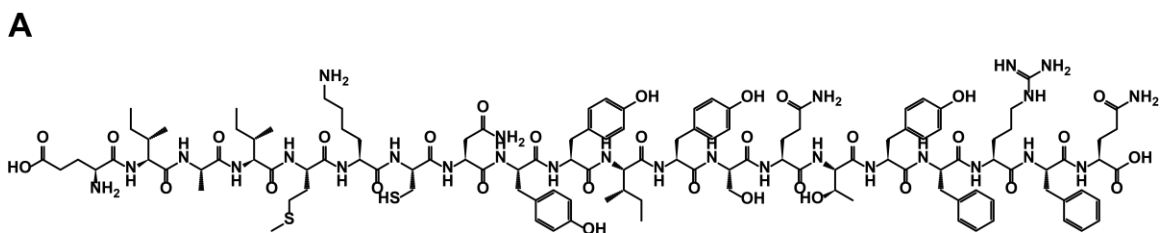


Figure S16. Characterization of EIA. (A) Chemical structure of EIA. (B) HPLC analysis of EIA. (C) Mass spectrum analysis of EIA.

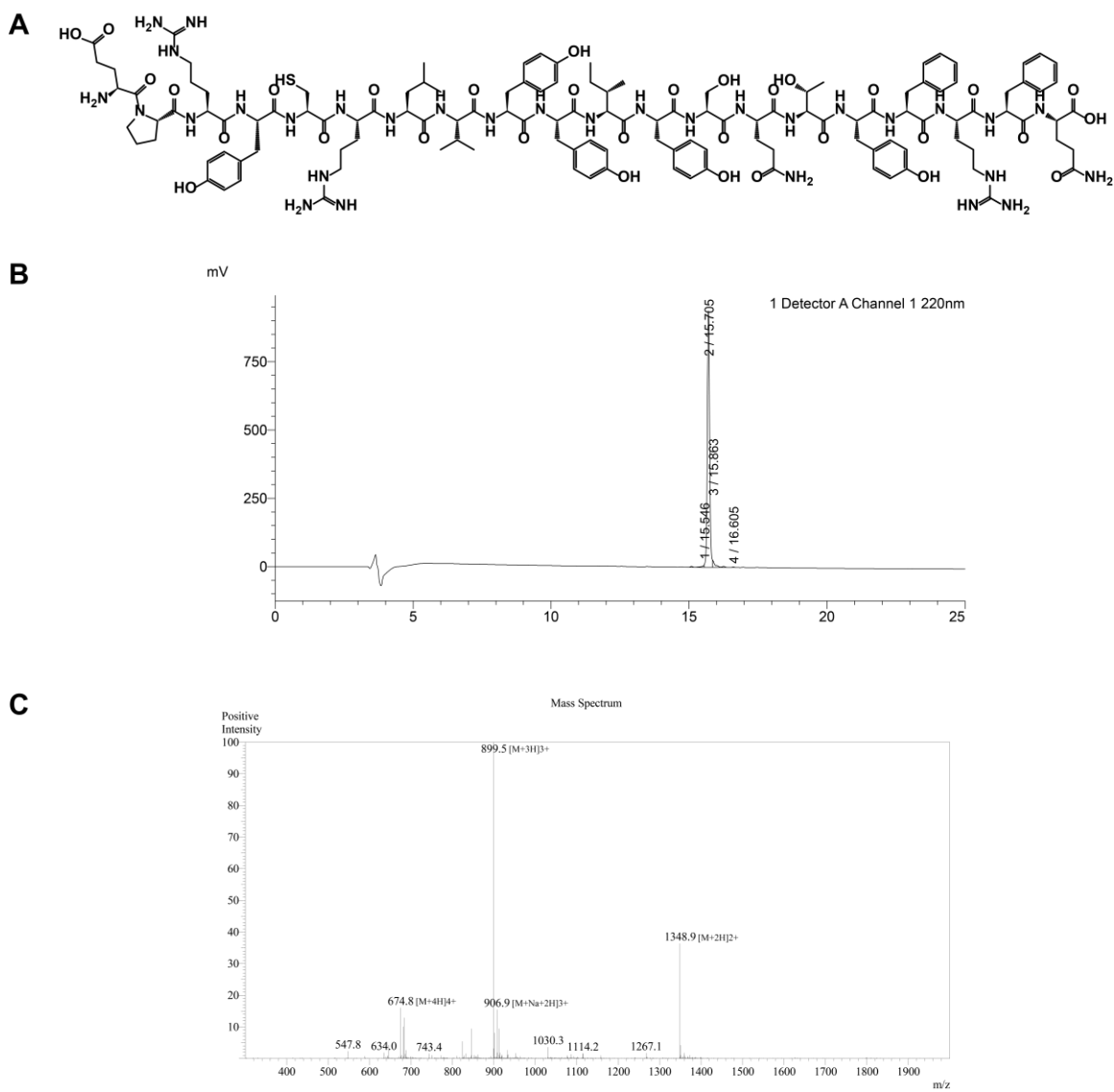


Figure S17. Characterization of **EPR**. (A) Chemical structure of **EPR**. (B) HPLC analysis of **EPR**. (C) Mass spectrum analysis of **EPR**.

3.2 Preparation and Characterization of Cy5-labeled Peptides

Peptide (**W10**, **AP**, **EIA**, or **EPR**, 4 mg) was dissolved in 1 mL of NaHCO_3 solution (pH 8.5~8.8), then 25 μL of Cy5-N-hydroxysuccinimide ester (CAS: 1358906-77-0, catalog number: S1060-1mg, brand: Solarbio) solution (10 mg/mL, in DMSO) was added, and the reaction was allowed to proceed overnight with magnetic stirring at 4°C in the dark. The reaction product was placed in a semi-permeable membrane (MWCO: 1000 Da) for dialysis against deionized water for 12 h, with water changes every 2 h. The solution was then concentrated under reduced pressure to obtain Cy5-labeled peptides. The identity and purity of each peptide were confirmed by analytical HPLC and high-resolution mass spectrometry (HRMS). For all peptides, the HPLC method was as follows: solvent A, 0.065% formic acid in 100% water; solvent B, 0.05% formic acid in 100% acetonitrile; 0 min-20 min, 30%-65% solvent B.

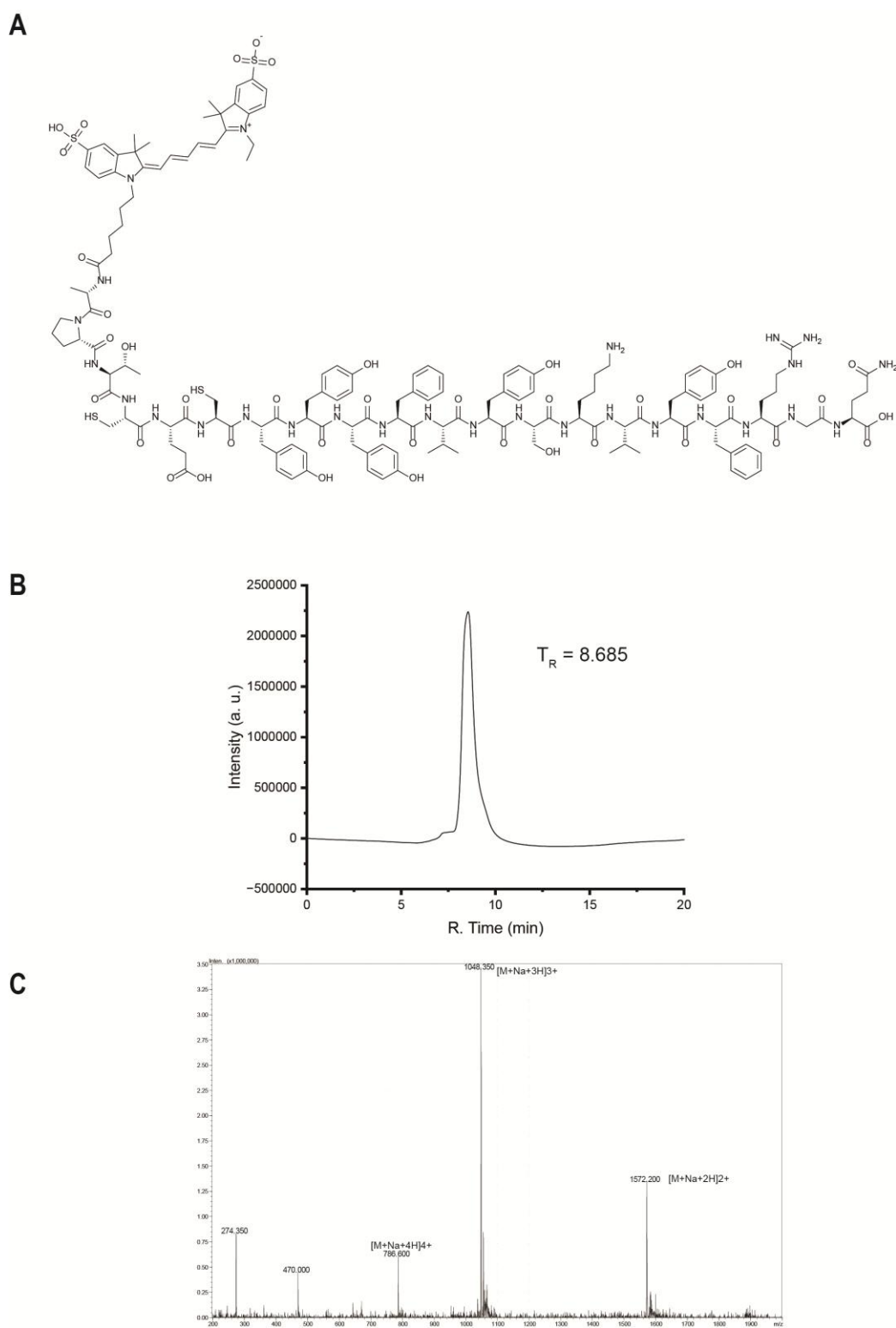


Figure S18. Characterization of **Cy5-AP**. (A) Chemical structure of **Cy5-AP**. (B) HPLC analysis of **Cy5-AP**. (C) Mass spectrum analysis of **Cy5-AP**.

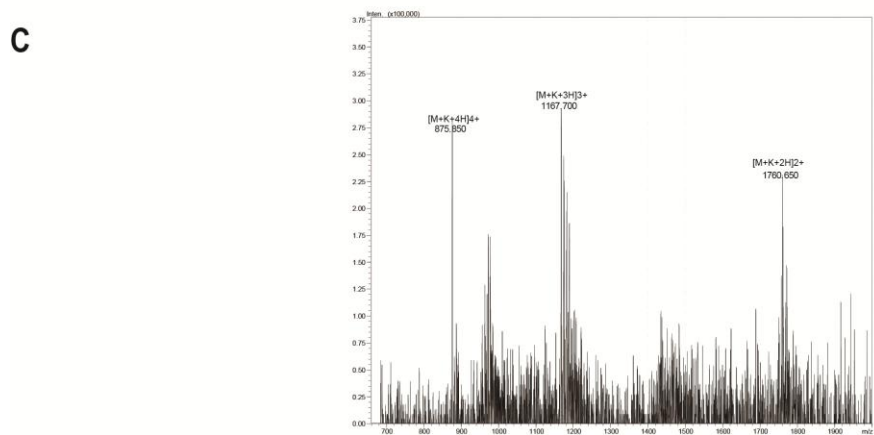
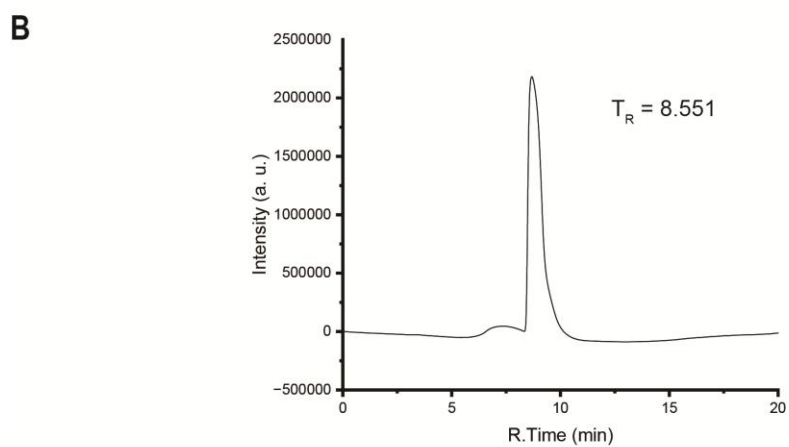
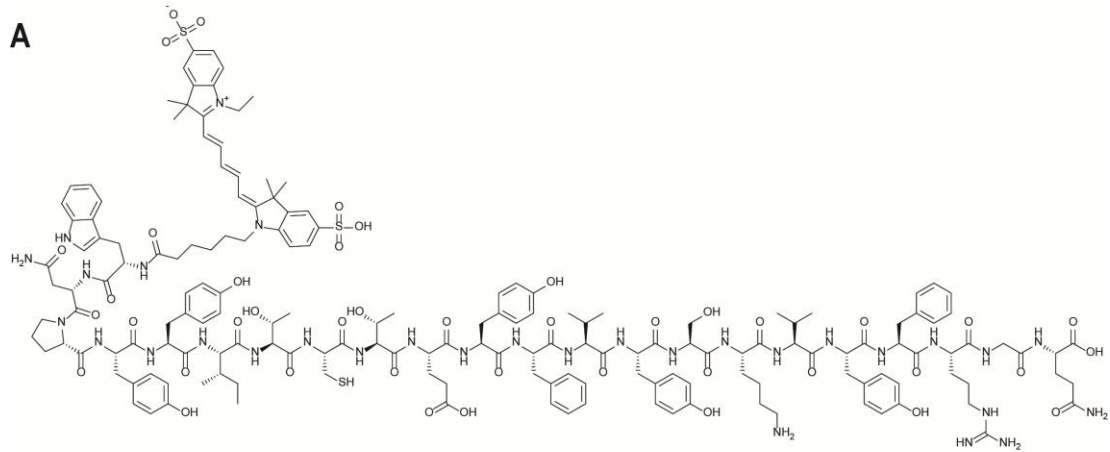
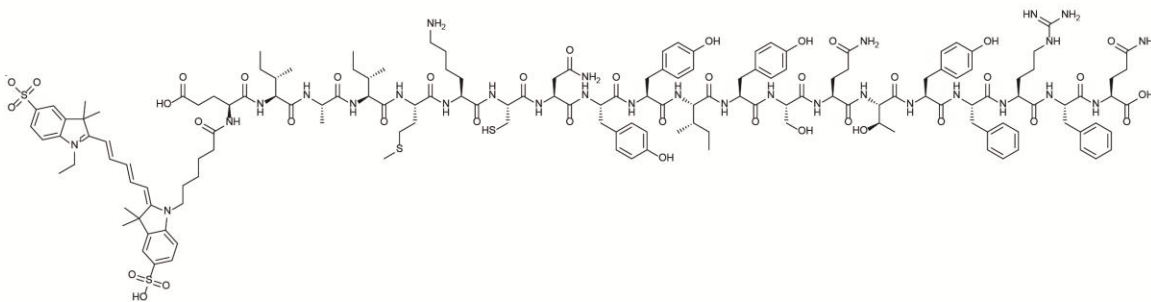
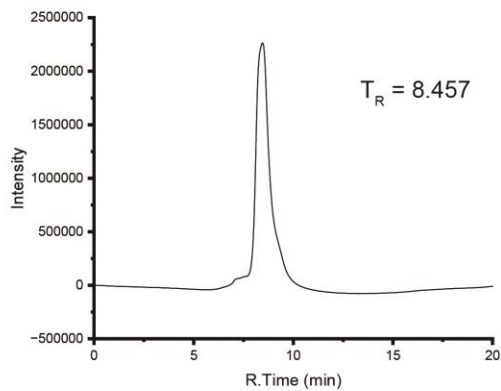


Figure S19. Characterization of **Cy5-W10**. (A) Chemical structure of **Cy5-W10**. (B) HPLC analysis of **Cy5-W10**. (C) Mass spectrum analysis of **Cy5-W10**.

A



B



C

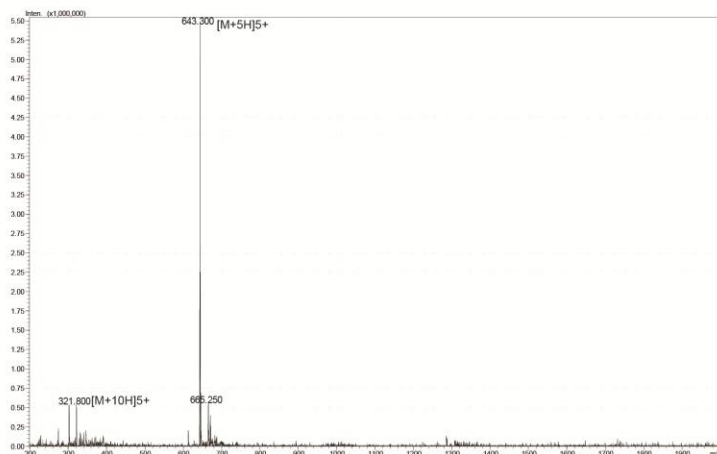


Figure S20. Characterization of **Cy5-EIA**. (A) Chemical structure of **Cy5-EIA**. (B) HPLC analysis of **Cy5-EIA**. (C) Mass spectrum analysis of **Cy5-EIA**.

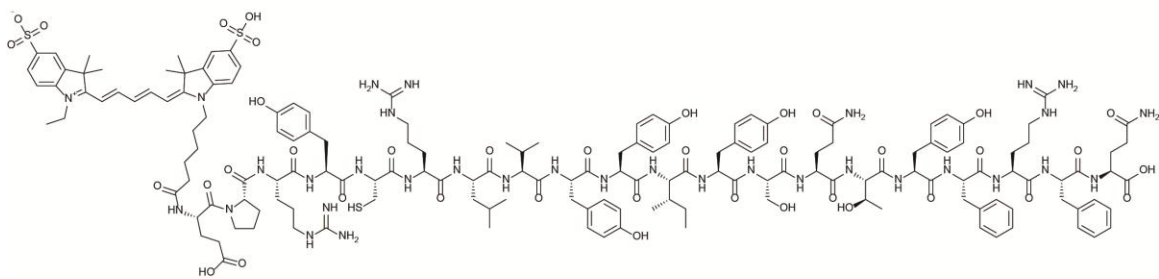
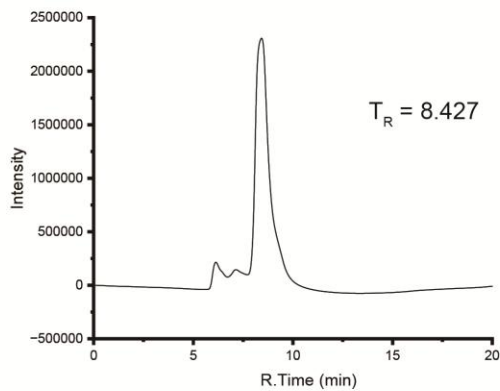
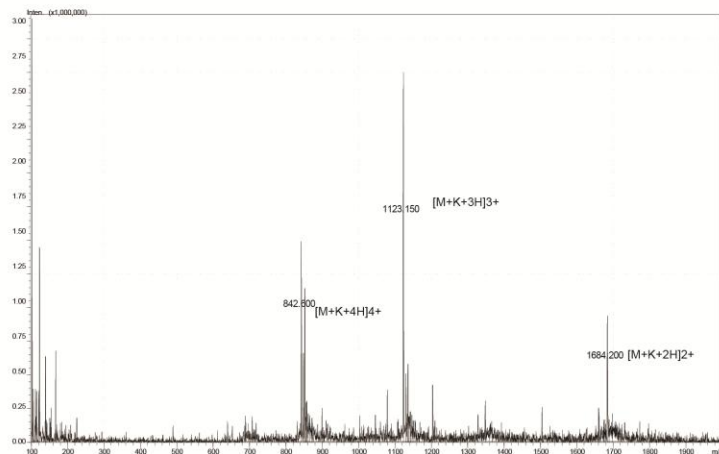
A**B****C**

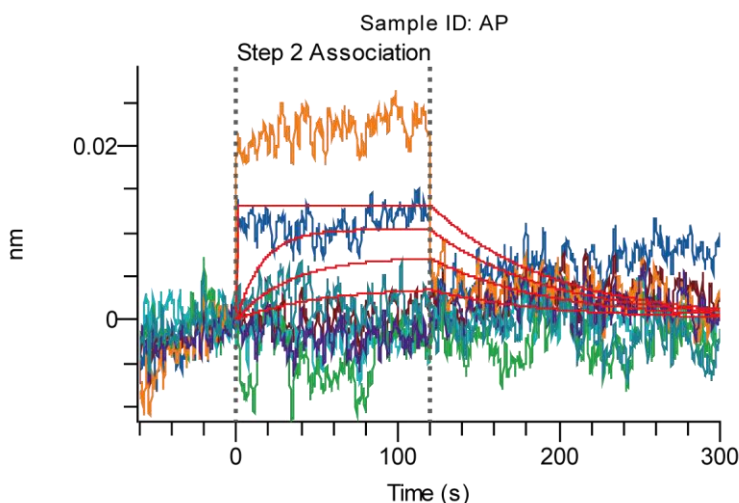
Figure S21. Characterization of **Cy5-EPR**. (A) Chemical structure of **Cy5-EPR**. (B) HPLC analysis of **Cy5-EPR**. (C) Mass spectrum analysis of **Cy5-EPR**.

4 Biophysical Characterization and Interaction Analysis

4.1 Bio-Layer Interferometry (BLI) Affinity Test

Binding affinities between peptides and recombinant death receptors were measured using an Octet RED96e system (ForteBio). Biotinylated recombinant human CD95 or DR5 extracellular domains (Sino Biological) were immobilized on streptavidin and Ni-NTA biosensors (loading concentration 5 $\mu\text{g/mL}$). Association and dissociation kinetics were measured using a series of peptide concentrations (1-1000 μM). Data were analyzed using ForteBio Data Analysis software (v11.0) with a 1:1 binding model to determine the kinetic parameters (k_{on} , k_{off}) and equilibrium dissociation constant (KD).

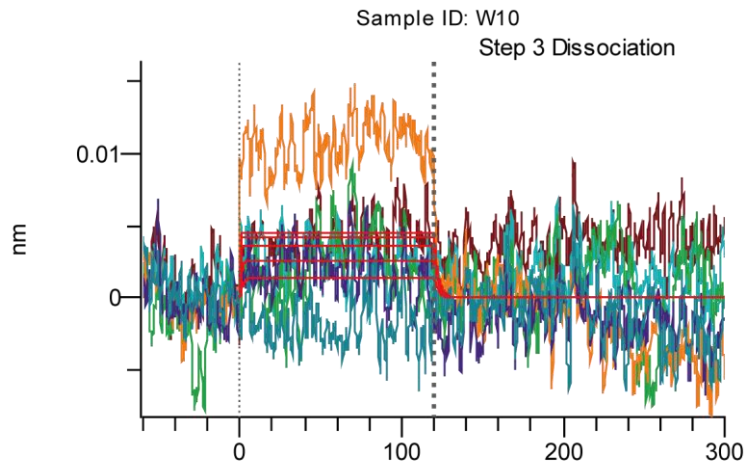
The binding kinetics of death receptors with peptide ligands assessed by Bio-layer Interferometry (BLI) are shown in Figure S7. The dose-response curves show the binding interactions between CD95 and peptide **AP** (Figure S22), CD95 and peptide **W10** (Figure S23), DR5 and peptide **EIA** (Figure S24), and DR5 and peptide **EPR** (Figure S25). Multiple concentrations of each peptide were tested to determine binding affinities and kinetic parameters. The curves represent global fitting of the experimental data to a 1:1 binding model.



Fitting Result

Index	Sensor Type	KD(M)	KD Error	ka (1/Ms)	ka Error	kdis (1/s)	kdis Error
1	Custom	1.37E-07	8.56E-09	9.89E04	5.17E03	1.35E-02	4.65E-04

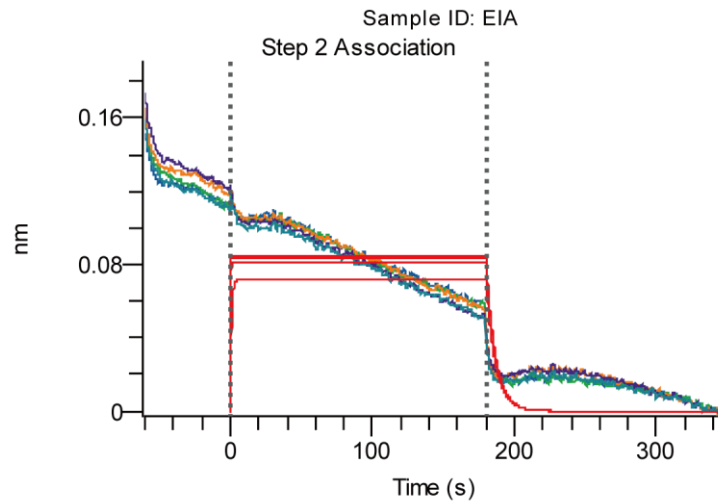
Figure S22. Binding kinetics of CD95 and peptide **AP** assessed by Biolayer Interferometry (BLI). Dose-response curves showing the binding interactions at multiple concentrations to determine binding affinities and kinetic parameters.



Fitting Result

Index	Sensor Type	KD(M)	KD Error	ka (1/Ms)	ka Error	kdis (1/s)	kdis Error
1	Custom	1.20E-07	3.43E-08	3.10E06	6.52E+05	3.73E-01	7.17E-02

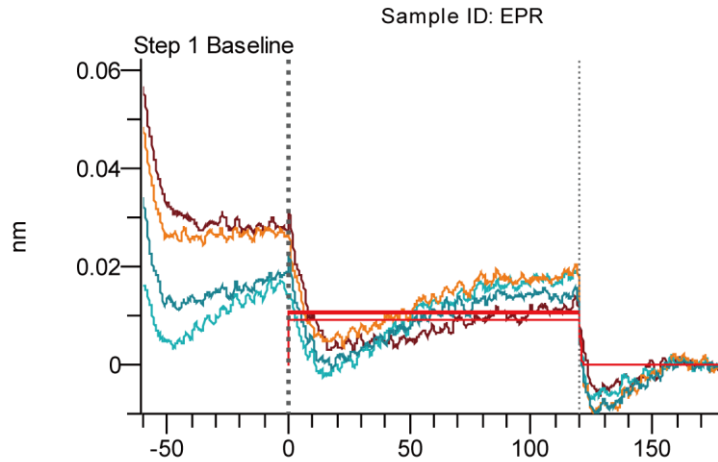
Figure S23. Binding kinetics of CD95 and peptide **W10** assessed by Bi-layer Interferometry (BLI). Dose-response curves showing the binding interactions at multiple concentrations to determine binding affinities and kinetic parameters.



Fitting Result

Index	Sensor Type	KD(M)	KD Error	ka (1/Ms)	ka Error	kdis (1/s)	kdis Error
1	Ni-NTA	4.20E-10	2.93E-11	3.55E08	2.21E07	1.49E-01	4.66E-03

Figure S24. Binding kinetics of DR5 and peptide **EIA** assessed by Bi-layer Interferometry (BLI). Dose-response curves showing the binding interactions at multiple concentrations to determine binding affinities and kinetic parameters.



Fitting Result

Index	Sensor Type	KD(M)	KD Error	ka (1/Ms)	ka Error	kdis (1/s)	kdis Error
1	Ni-NTA	1.70E-09	8.53E-10	1.37E09	5.15E08	2.33E00	7.71E-01

Figure S25. Binding kinetics of DR5 and peptide EPR assessed by Biolayer Interferometry (BLI). Dose-response curves showing the binding interactions at multiple concentrations to determine binding affinities and kinetic parameters.

4.2 Circular Dichroism (CD) Spectroscopy

CD spectra were recorded on a Jasco J-815 spectropolarimeter using a 0.1 cm path length quartz cuvette. Peptides were dissolved in 10 mM phosphate buffer (pH 7.4) at concentrations ranging from 1.25 to 40.0 μM . Spectra were recorded from 190 to 260 nm at 20°C with a scanning speed of 100 nm/min, a bandwidth of 1 nm, and a response time of 1 s. For each sample, five scans were averaged, and the buffer background was subtracted. For receptor binding studies, spectra were recorded in the presence of recombinant CD95 or DR5 extracellular domains at varying concentrations (Figure S26-S32). Quantitative secondary structure analysis was performed using BeStSel¹ software to determine the percentage of α -helix, β -sheet, β -turn, and random coil structures.

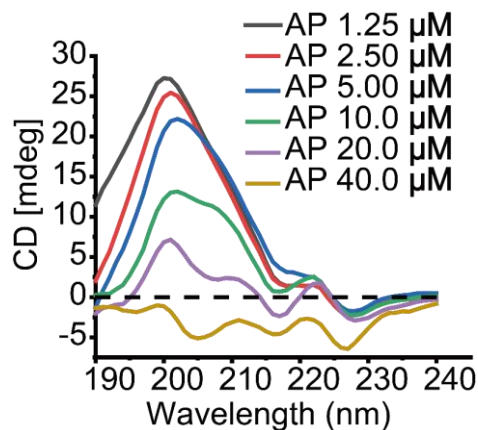


Figure S26. Circular dichroism spectra of AP without CD95 protein at concentrations ranging from 1.25 to 40.0 μM .

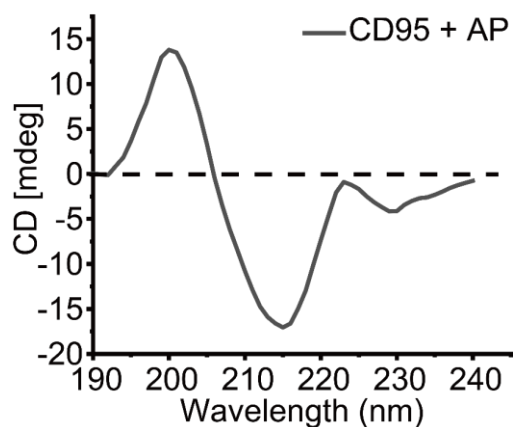


Figure S27. Circular dichroism spectra of **AP** (40.0 μM) alone and in complex with CD95 protein (**AP**: CD95 molar ratio = 500:1).

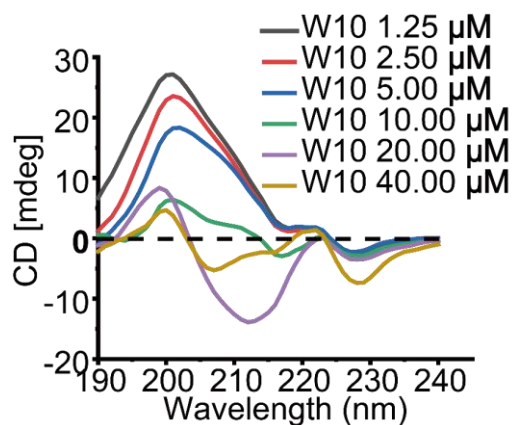


Figure S28. Circular dichroism spectra of **W10** without CD95 protein at concentrations ranging from 1.25 to 40.0 μM .

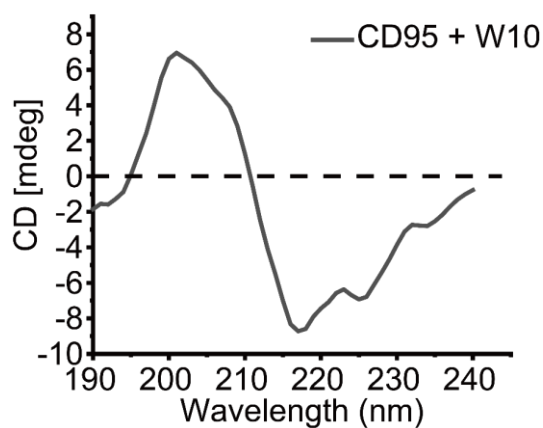


Figure S29. Circular dichroism spectra of **W10** (40.0 μM) alone and in complex with CD95 protein (**W10**: CD95 molar ratio = 500:1).

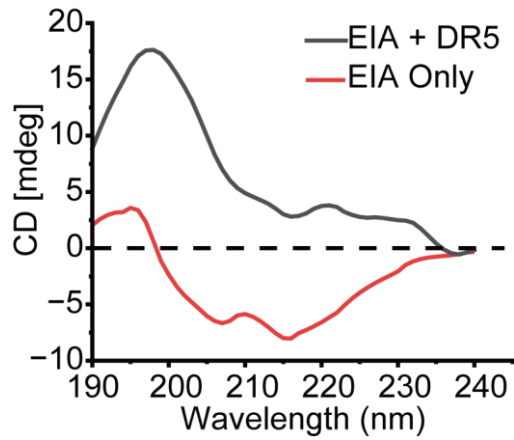


Figure S30. Circular dichroism spectra of EIA (40.0 μ M) alone and in complex with DR5 protein (EIA: DR5 molar ratio = 500:1).

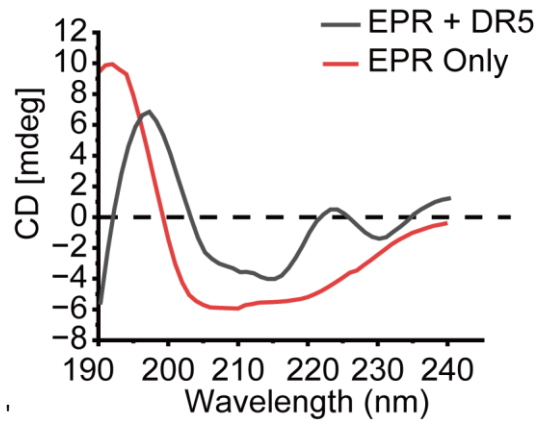


Figure S31. Circular dichroism spectra of EPR (40.0 μ M) alone and in complex with DR5 protein (EPR: DR5 molar ratio = 500:1).

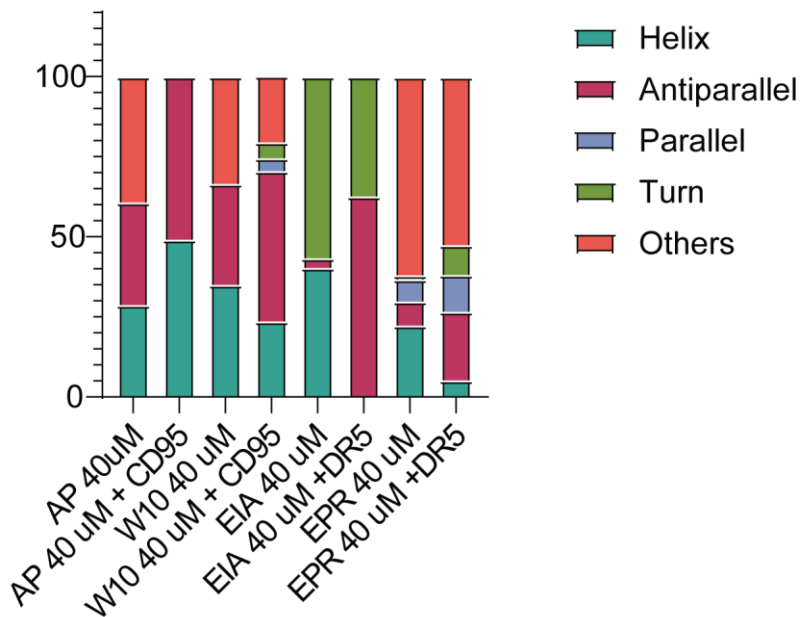


Figure S32. Quantification of different secondary structure content of **AP** and **W10** with/without CD95 and **EIA** and **EPR** with/without DR5 at the molar ratio of 500:1 (peptide concentration: 40.0 μ M).

4.3 Immunoprecipitation and Size Exclusion Chromatography

HT29 cells were treated with peptides (40 or 80 μ M) for 12 hours, then lysed in ice-cold lysis buffer (50 mM Tris-HCl pH 7.4, 150 mM NaCl, 1% Triton X-100, 0.5% sodium deoxycholate, protease inhibitor cocktail). Cell lysates were pre-cleared with Protein G Sepharose beads and non-specific IgG for 1 hour at 4°C. Immunoprecipitation was performed using anti-CD95 monoclonal antibody (**APO-1**, Enzo Life Sciences) overnight at 4°C, followed by incubation with Protein G beads for 2 hours. Immunoprecipitates were washed four times with lysis buffer, eluted with 0.1 M glycine (pH 2.5), and neutralized with 1 M Tris-HCl (pH 8.0). Size exclusion chromatography was performed on a Superdex 200 Increase 10/300 GL column (GE Healthcare) equilibrated with PBS at a flow rate of 0.5 mL/min. Protein elution was monitored by absorbance at 280 nm.

5 Cell Viability Assay

5.1 General Information

HT29 (human colorectal adenocarcinoma), COLO205 (human colorectal adenocarcinoma), and MDA-MB-231 (human breast adenocarcinoma) cancer cell lines were obtained from ATCC and cultured in DMEM (for MDA-MB-231) or RPMI-1640 (for HT29 and COLO205) supplemented with 10% FBS, 100 U/mL penicillin, and 100 μ g/mL streptomycin. HEK293 (human embryonic kidney) cells were also obtained from ATCC and cultured in DMEM with the same supplements. All cells were maintained at 37°C in a humidified atmosphere with 5% CO₂ and were routinely tested for mycoplasma contamination.

5.2 CTG Assay of AP, W10, EIA and EPR

Cell viability was assessed using the CellTiter-Glo Luminescent Cell Viability Assay (Promega). HT-29, COLO205, MDA-MB-231 and HEK293 cells were seeded in 96-well white opaque plates (5,000 cells/well) and allowed to attach overnight. Cells were then treated with various concentrations of peptides (0.1-160 μ M) for 48 hours in triplicate (n=3). After treatment, an equal volume of CellTiter-Glo reagent was added to each well, and luminescence was measured using a SpectraMax M5 plate reader (Molecular Devices) after 10 minutes of incubation. IC₅₀ values were calculated using GraphPad Prism 10.0 software with the dose-response inhibitor four-parameter nonlinear regression model. Error bars represent the standard deviation of three independent experiments.

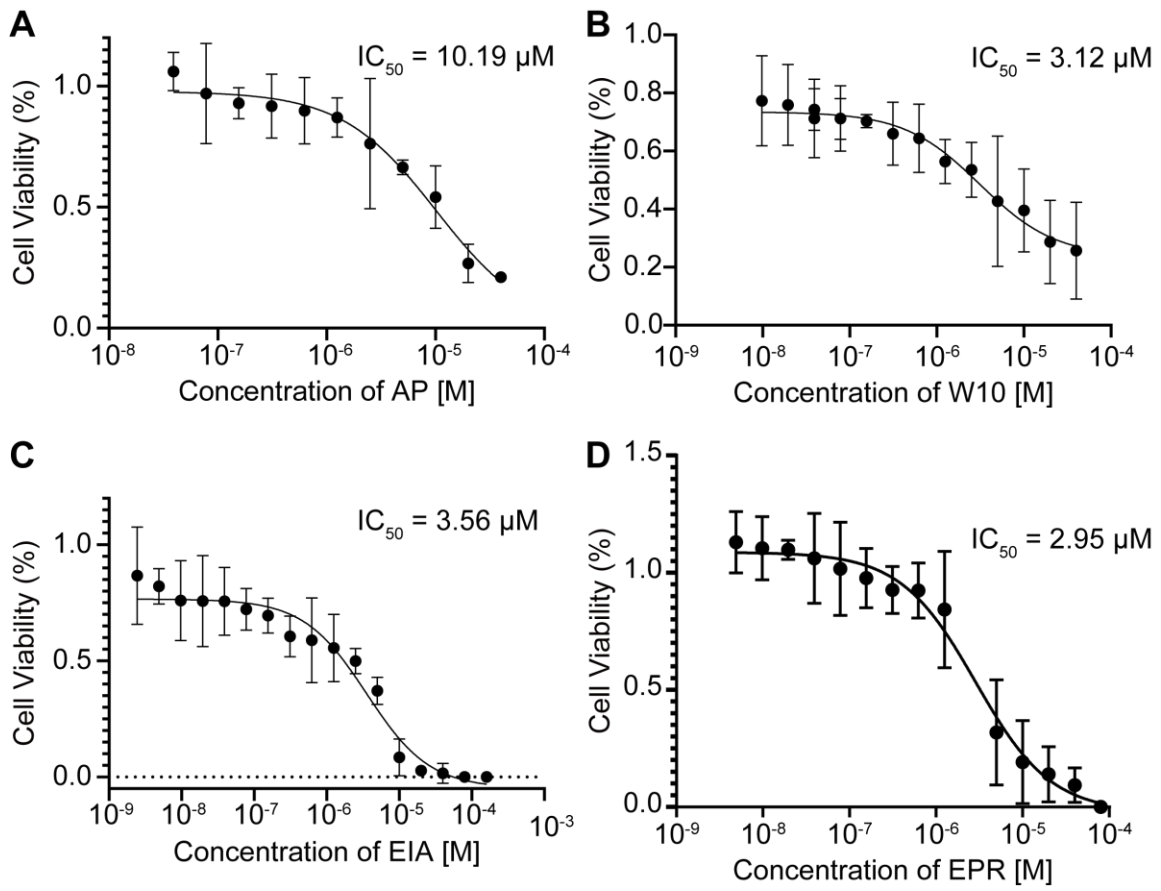


Figure S33. Dose-dependent cytotoxicity of peptides **AP** (A), **W10** (B), **EIA** (C), and **EPR** (D) in HT-29 cells after 48h treatment.

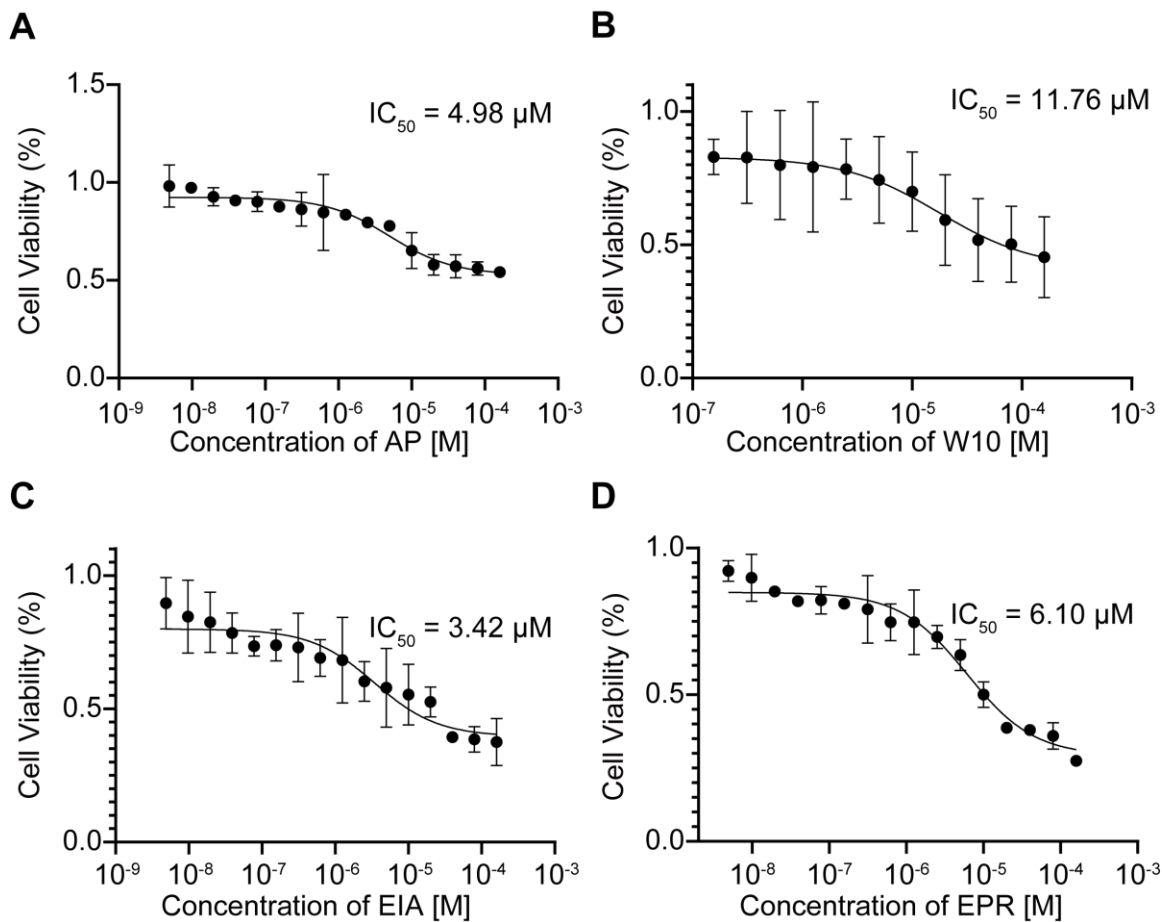


Figure S34. Dose-dependent cytotoxicity of peptides **AP** (A), **W10** (B), **EIA** (C), and **EPR** (D) in COLO205 cells after 48h treatment.

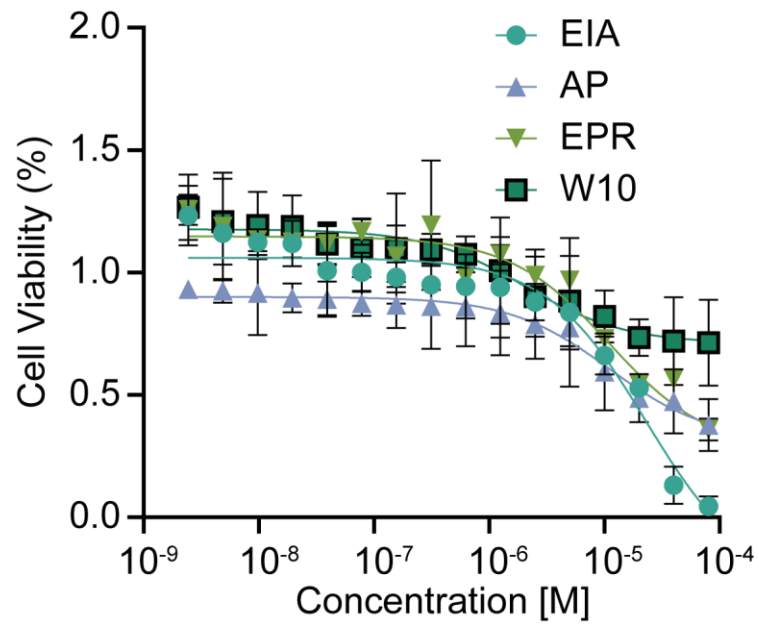


Figure S35. Dose-dependent cytotoxicity of peptides AP (A), W10 (B), EIA (C), and EPR (D) in MDA-MB-231 cells after 48h treatment.

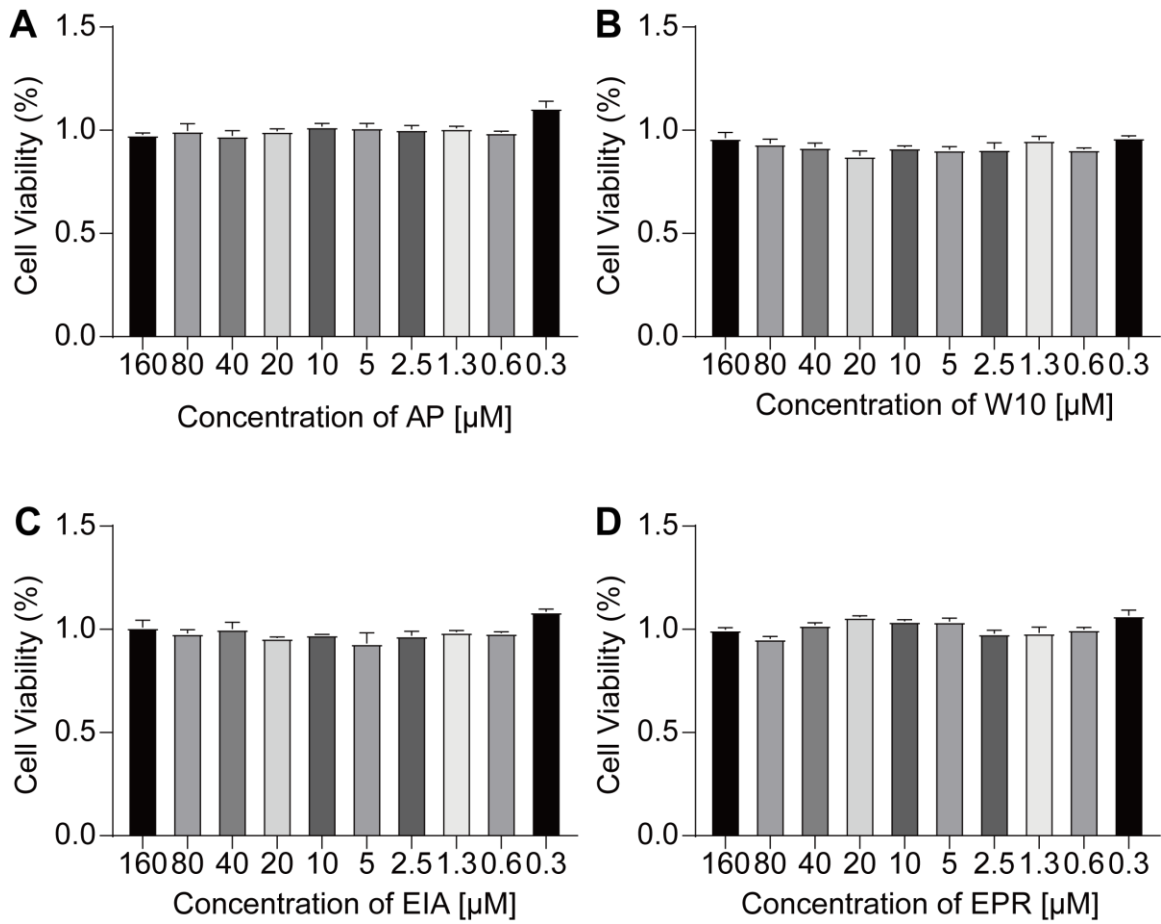


Figure S36. Dose-dependent cytotoxicity of peptides **AP** (A), **W10** (B), **EIA** (C), and **EPR** (D) in HEK293 cells after 48h treatment.

6 Confocal Microscopy

6.1 Plasmid Construction and Transfection

CD95-GFPspark (#HG10217-ACG), DR5-GFPspark (#HG10465-ACG) and NF- κ B-GFPspark (#HG12054-ANG) were purchased from Sino Biological. All plasmids were verified by DNA sequencing. Transient transfections were performed using Lipofectamine 2000 (Invitrogen) according to the manufacturer's instructions. Briefly, cells were seeded in appropriate plates 24 hours before transfection to reach 70-80% confluence at the time of transfection. Plasmid DNA (1-2 μ g) and Lipofectamine 2000 were diluted in Opti-MEM, mixed, and incubated for 15 minutes at room temperature before adding to cells.

6.2 Confocal Microscopy for colocalization and NF- κ B translocation

For colocalization studies, HeLa cells transfected with CD95-GFPspark or DR5-GFPspark were seeded into glass-bottom dishes at a density of 1×10^5 cells per well in DMEM medium overnight. After 24 hours, cells were treated with Cy5-labeled peptides (10 μ M) for 6 hours, washed with PBS. The cellular imaging was performed by Confocal laser scanning microscopy (CLSM). For NF- κ B translocation studies, HeLa cells transfected with NF- κ B-GFPspark were treated with peptides at indicated concentrations (5-10 μ M) for various time periods (24-48 hours). Images were acquired using a Leica TCS SP8 confocal microscope with a 63 \times oil immersion objective. Hoechst 33342 (1 mg/mL; Life Technologies) was used to stain the nucleus of cells at 37°C for 10 min.

6.3 Nuclear Localization of CD95

The observation that **AP** and **W10** peptides colocalized with CD95 primarily in nuclei rather than membranes represents an intriguing deviation from the canonical understanding of death receptor biology. Traditionally, CD95 is described as a type I transmembrane protein primarily localized to the plasma membrane where it initiates extrinsic apoptotic signaling. Our findings suggest a potential alternative trafficking pathway triggered by our peptide agonists. This nuclear translocation likely represents a multi-step process wherein peptide binding initiates receptor internalization followed by nuclear import, possibly through recognition of cryptic nuclear localization signals exposed upon conformational changes induced by our β -sheet scaffolds. Previous studies have identified non-canonical roles for internalized death receptors, including nuclear translocation of cleaved receptor fragments that may directly influence gene expression patterns. This nuclear localization differs fundamentally from the classical death-inducing signaling complex (DISC) formation at the plasma membrane and may represent an additional mechanism through which our peptides exert their effects. The therapeutic implications of this nuclear localization are significant, potentially enabling our peptides to bypass membrane-associated resistance mechanisms that often limit the efficacy of conventional death receptor agonists.

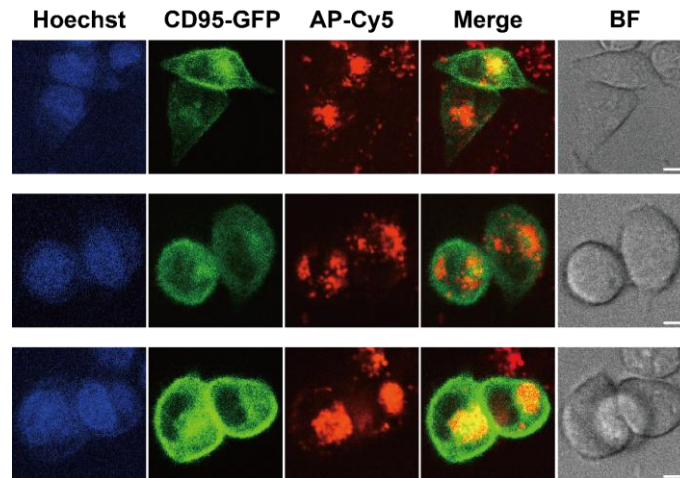


Figure S37. Subcellular localization and co-localization analysis of CD95-GFPspark with **AP**-Cy5. Representative confocal microscopy images showing the distribution in HeLa cells. Nuclei were stained with Hoechst 33342 (blue). GFP-tagged proteins are shown in green, Cy5-labeled **AP** in red, and regions of co-localization appear yellow in merged images. Brightfield (BF) images show cell morphology. Three representative cells are shown. Scale bar: 10 μ m.

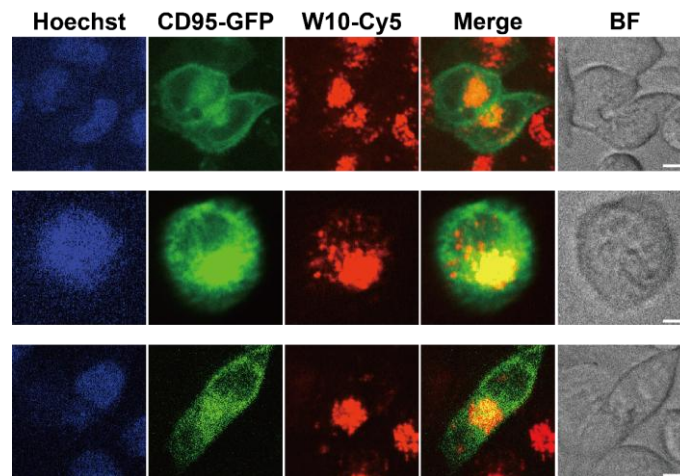


Figure S38. Subcellular localization and co-localization analysis of CD95-GFPspark with **W10**-Cy5. Representative confocal microscopy images showing the distribution in HeLa cells. Nuclei were stained with Hoechst 33342 (blue). GFP-tagged proteins are shown in green, Cy5-labeled **W10** in red, and regions of co-localization appear yellow in merged images. Brightfield (BF) images show cell morphology. Three representative cells are shown. Scale bar: 10 μ m.

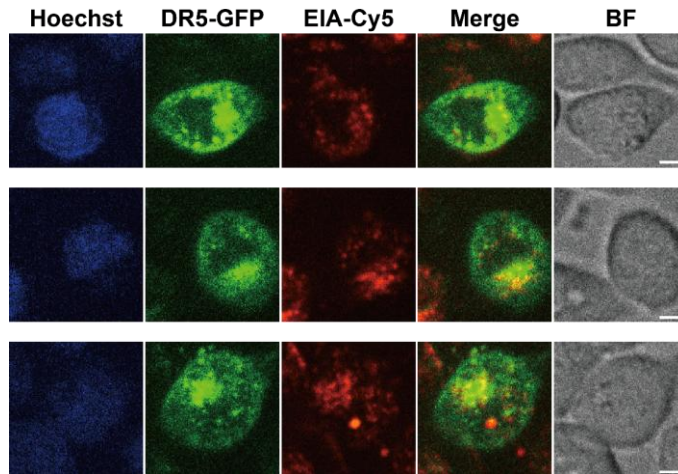


Figure S39. Subcellular localization and co-localization analysis of DR5-GFPspark with EIA-Cy5. Representative confocal microscopy images showing the distribution in HeLa cells. Nuclei were stained with Hoechst 33342 (blue). GFP-tagged proteins are shown in green, Cy5-labeled EIA in red, and regions of co-localization appear yellow in merged images. Brightfield (BF) images show cell morphology. Three representative cells are shown. Scale bar: 10 μ m.

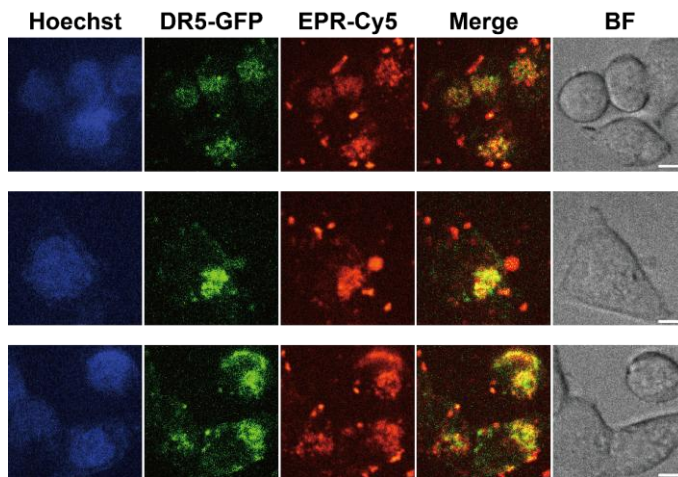


Figure S40. Subcellular localization and co-localization analysis of DR5-GFPspark with EPR-Cy5. Representative confocal microscopy images showing the distribution in HeLa cells. Nuclei were stained with Hoechst 33342 (blue). GFP-tagged proteins are shown in green, Cy5-labeled EPR in red, and regions of co-localization appear yellow in merged images. Brightfield (BF) images show cell morphology. Three representative cells are shown. Scale bar: 10 μ m.

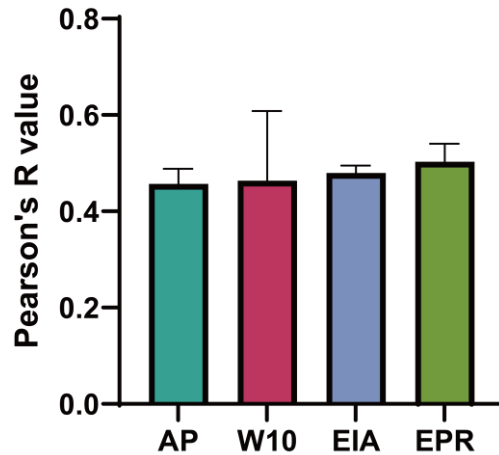


Figure S41. Quantitative assessment of colocalization between Cy5-labeled peptides **AP** and **W10** with CD95-GFPspark, and between **EIA**, **EPR** with DR5-GFPspark using Pearson correlation analysis (n=3).

6.4 NF- κ B Activation and Apoptotic Signaling

The observed nuclear translocation of NF- κ B following treatment with our peptide agonists presents an apparent paradox, as NF- κ B signaling is traditionally associated with pro-survival functions, while our peptides demonstrate clear pro-apoptotic effects. This apparent contradiction can be reconciled through understanding the biphasic nature of NF- κ B signaling in death receptor cascades. Initial activation of NF- κ B following death receptor engagement represents an early stress response that precedes commitment to cell death. This transient NF- κ B activation can upregulate pro-apoptotic proteins including death receptors themselves, thereby amplifying the initial apoptotic signal in a positive feedback loop. Notably, similar NF- κ B activation pathways are observed in the oligomerization of other TNFR superfamily members, such as OX40 (CD134), which utilizes TRAF-dependent signaling to activate NF- κ B. The key difference lies in the cellular context and the simultaneous activation of additional signaling pathways; while OX40 oligomerization primarily promotes survival in immune cells, our peptide-induced receptor clustering leads to apoptosis in cancer cells due to concurrent activation of death domains. Additionally, sustained NF- κ B activation in the context of simultaneous strong pro-apoptotic signals (as generated by our peptide agonists) can lead to a phenomenon known as "nuclear factor overload," wherein excessive transcriptional activity triggers cellular stress responses that ultimately favor apoptosis over survival. Our data suggests that the peptide-induced NF- κ B translocation contributes to, rather than counteracts, the apoptotic cascade through altered transcriptional programming that shifts the balance of pro- and anti-apoptotic factors in treated cells.

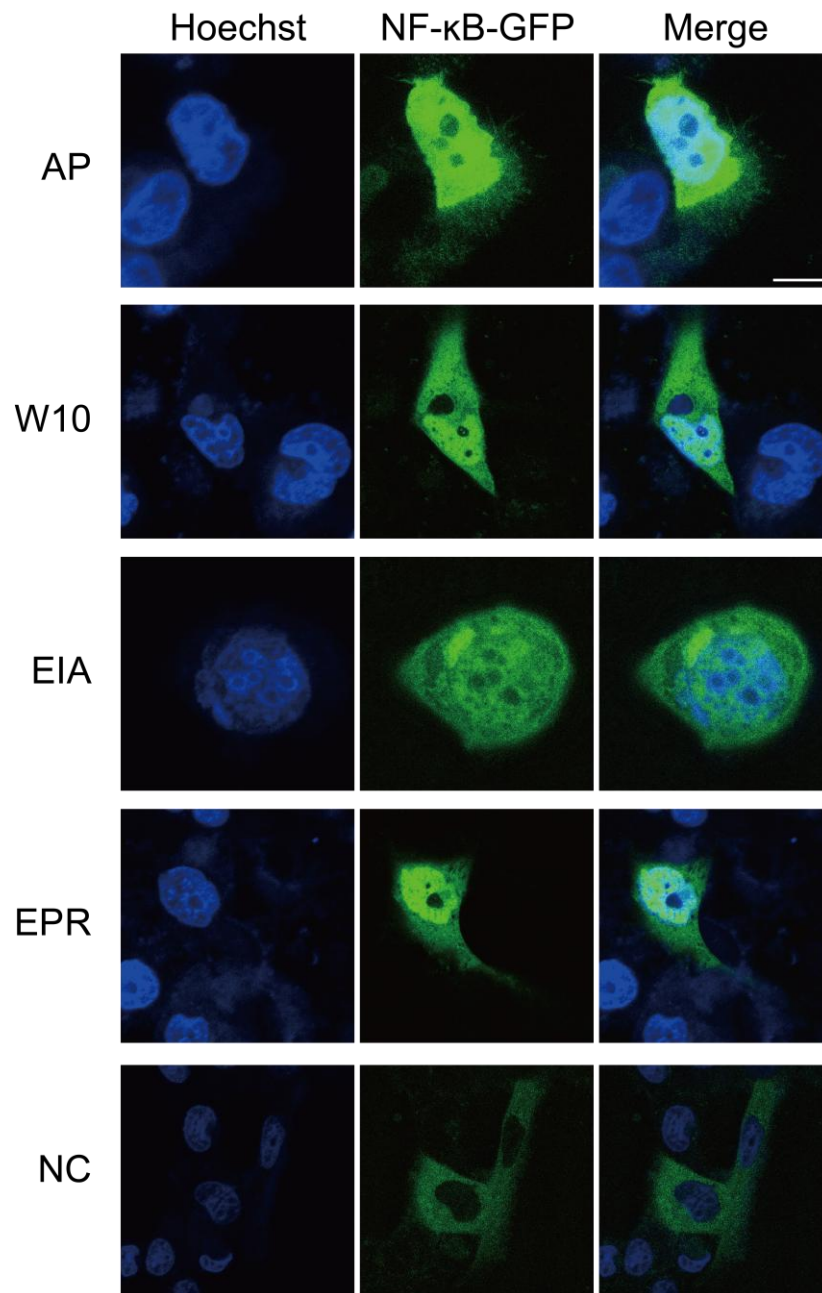


Figure S42. Representative CLSM images of NF-kappaB-GFPspark plasmid transfected HeLa cells after incubation with **AP**, **W10**, **EIA** and **EPR** for 12 h. Scale Bar: 10 μ m.

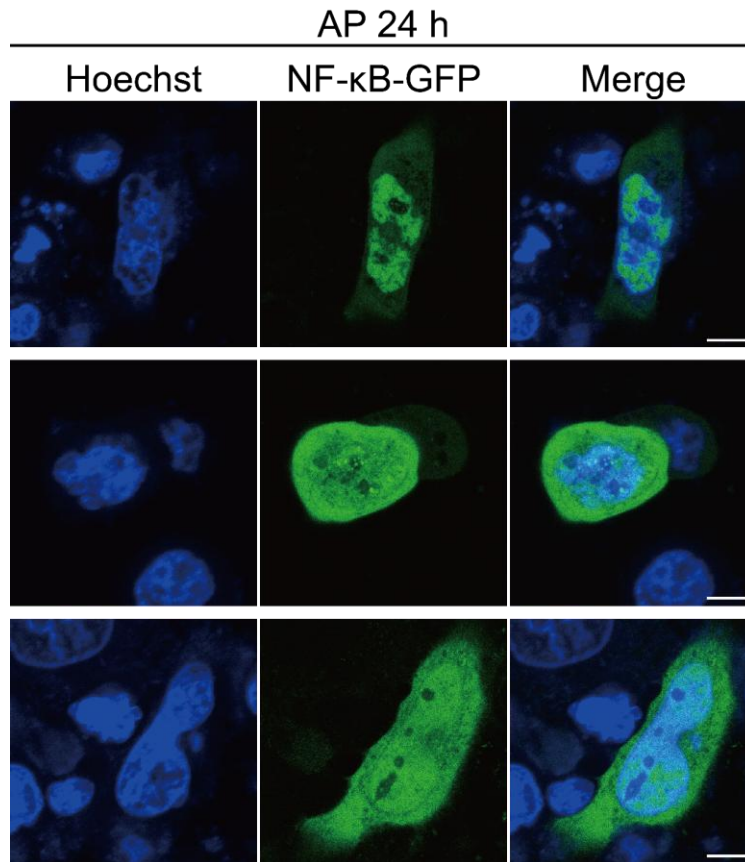


Figure S43. Nuclear translocation of NF- κ B-GFP in response to AP treatment over 24 hours. Confocal microscopy images showing the subcellular localization of NF- κ B-GFPspark (green) in cells treated for 24 hours. Nuclei were stained with Hoechst 33342 (blue). Merged images demonstrate the degree of nuclear translocation of NF- κ B-GFP. Three representative cells are shown. Scale bars: 10 μ m.

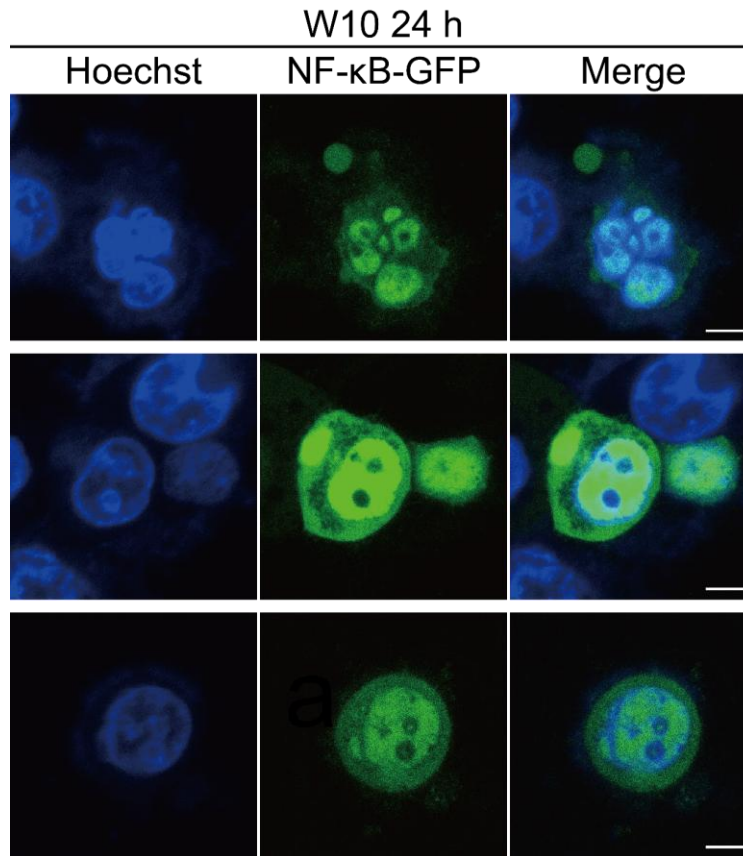


Figure S44. Nuclear translocation of NF- κ B-GFP in response to **W10** treatment over 24 hours. Confocal microscopy images showing the subcellular localization of NF- κ B-GFP (green) in cells treated for 24 hours. Nuclei were stained with Hoechst 33342 (blue). Merged images demonstrate the degree of nuclear translocation of NF- κ B-GFP. Three representative cells are shown. Scale bars: 10 μ m.

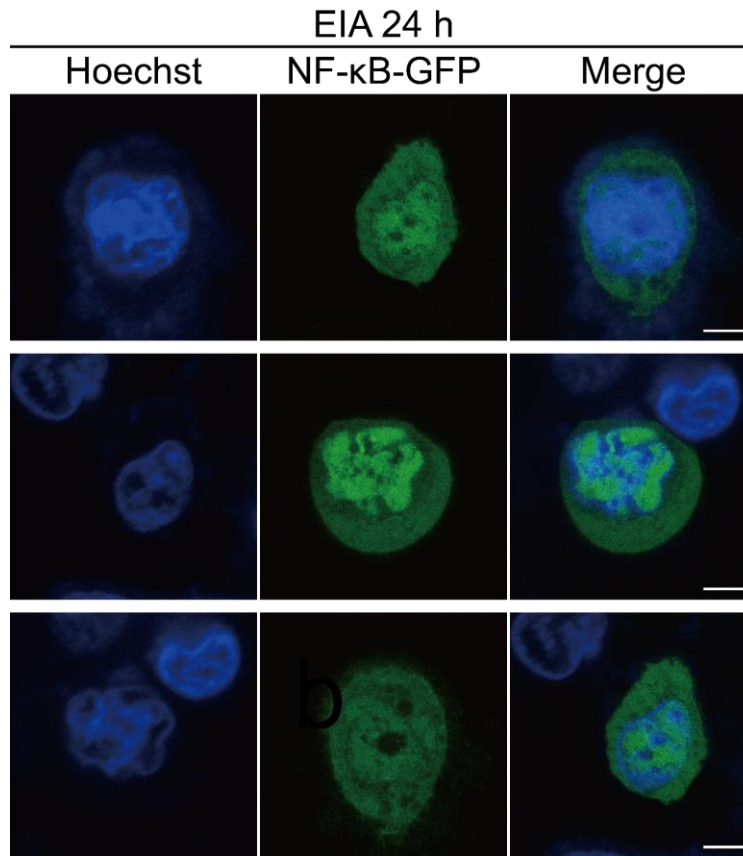


Figure S45. Nuclear translocation of NF- κ B-GFP in response to **EIA** treatment over 24 hours. Confocal microscopy images showing the subcellular localization of NF- κ B-GFP (green) in cells treated for 24 hours. Nuclei were stained with Hoechst 33342 (blue). Merged images demonstrate the degree of nuclear translocation of NF- κ B-GFP. Three representative cells are shown. Scale bars: 10 μ m.

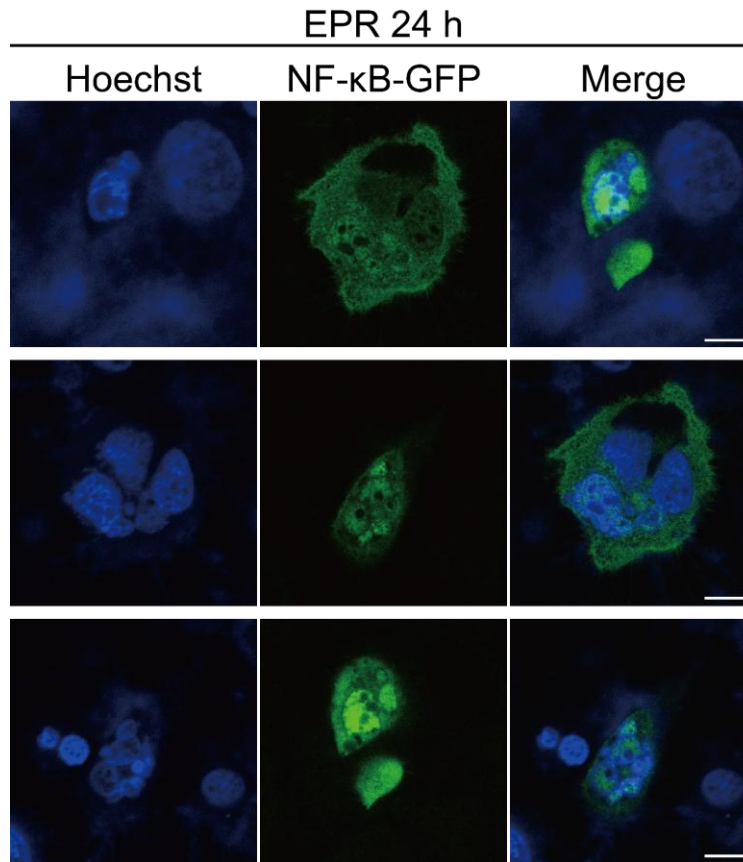


Figure S46. Nuclear translocation of NF-κB-GFP in response to EPR treatment over 24 hours. Confocal microscopy images showing the subcellular localization of NF-κB-GFP (green) in cells treated for 24 hours. Nuclei were stained with Hoechst 33342 (blue). Merged images demonstrate the degree of nuclear translocation of NF-κB-GFP. Three representative cells are shown. Scale bars: 10 μm.

One-way ANOVA analysis of NF-κB nuclear translocation in peptide-treated NF-κB-GFPspark HeLa cells

Tukey's multiple comparisons test	Mean Diff	95,00% CI of diff	Significant?	Summary	Adjusted P Value
NC vs. AP	-0.6667	-0.8799 to -0.4534	Yes	****	<0.0001
NC vs. W10	-0.2833	-0.4966 to -0.07005	Yes	**	0.0097
NC vs. EIA	-0.5400	-0.7533 to -0.3267	Yes	****	<0.0001
NC vs. EPR	-0.1867	-0.3999 to 0.02661	No	ns	0.0939

7 Apoptosis Assay and Immunoblotting

7.1 Apoptosis Assay

Annexin V-FITC Apoptosis Detection Kit is a cell apoptosis detection kit used to detect phosphatidylserine that appears on the cell membrane surface during apoptosis. By using flow cytometry instrument to check the experimental results. COLO205 cells were first cultured in 6-well plates and adhered. **AP**, **W10**, **EIA** and **EPR** were incubated with cells for 24 h or 48 h. Each sample was added to 2 mL centrifuge tube, washed with PBS, and centrifuged. Buffer (1×) 200 μL was added to the centrifuge tube. After mixing,

Annexin V-FITC (10 μ L) was added to each tube. Finally, 5 μ L of PI to each centrifuge tube were add and conduct the test.

7.2 Immunoblotting

The pretreated cells were re-suspended by the lysis buffer which contains 50 mM Tris-HCl (pH 8.0), 150 mM NaCl, 1% (v/v) Triton-X 100 and protease inhibitor. BCA kit (Beyotime) was utilized to estimate the protein content. Each sample (35 μ g of protein) was loaded to the SDS-PAGE and then transferred to 45 μ m PVDF membrane. The blots were blocked in blocking buffer which contains 5% (wt/v) non-fat milk, 0.1% (v/v) Tween-20 in 10 mM TBS. After washing three times with TBST buffer (10 mM TBS containing 0.1% (v/v) Tween-20), the blots were incubated with primary antibodies against cleaved caspase-3 (Asp175) (Cell Signaling Technology, Beverly, MA, USA, #9661S, 1:1000 dilution) and β -actin (Abcam, Cambridge, UK, ab8226, 1:4000 dilution) at 4 $^{\circ}$ C on a shaker for 16 h. Then after washing with TBST buffer for another 3 times, the blots were incubated with secondary antibody for 2 h at room temperature on a shaker. After washing with TBST buffer for 3 times, the blots were subsequently scanned on a Typhoon Trio Variable Mode Imager.

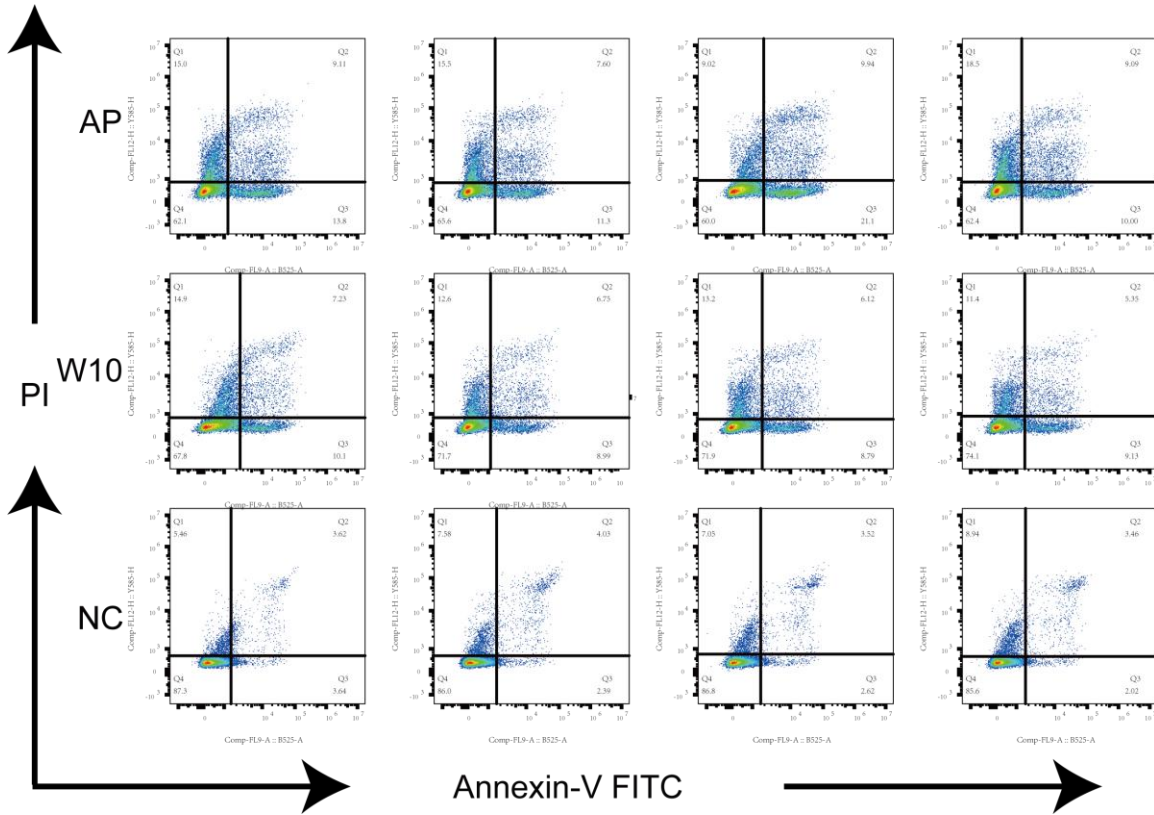


Figure S47. Flow cytometry analysis of COLO205 cell apoptosis following 24 h treatment with AP (10 μ M) and W10 (10 μ M). Apoptosis detection by ANNEXIN V-FITC/PI double staining. NC, negative control.

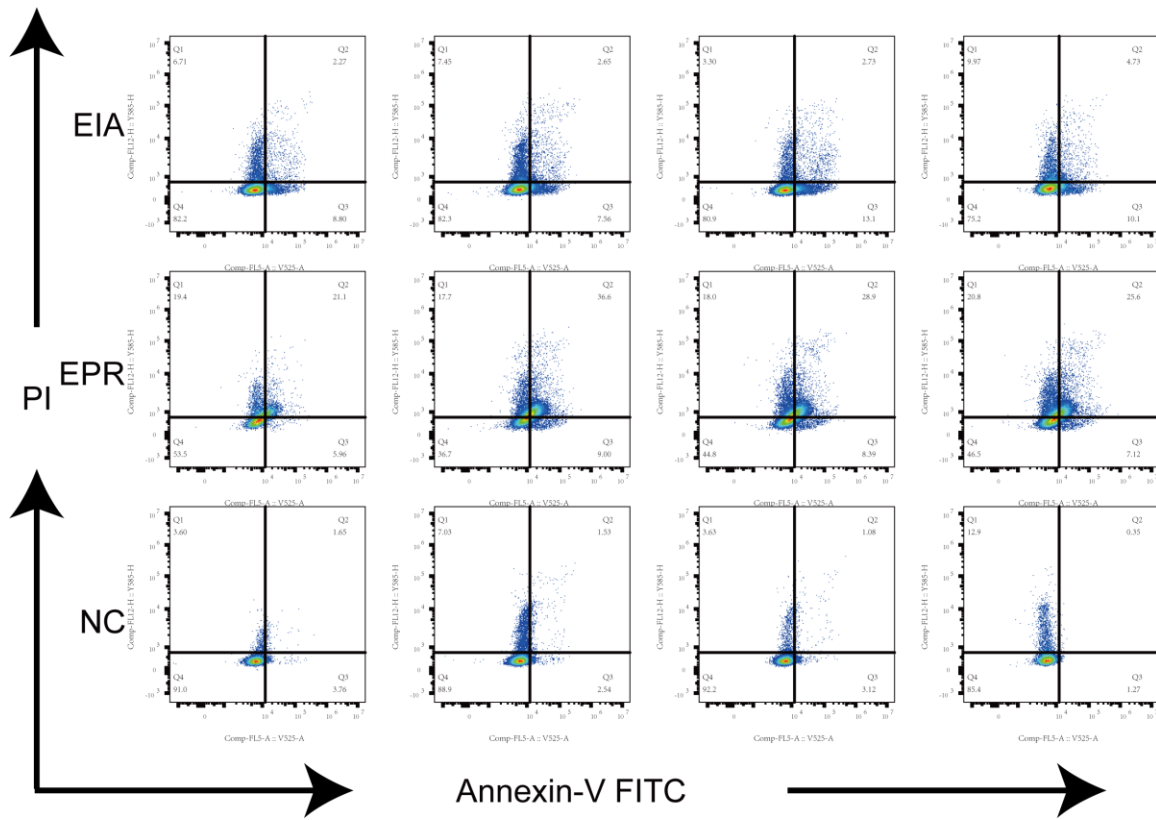


Figure S48. Flow cytometry analysis of COLO205 cell apoptosis following 24 h treatment with EIA (10 μ M) and EPR (10 μ M). Apoptosis detection by ANNEXIN V-FITC/PI double staining. NC, negative control.

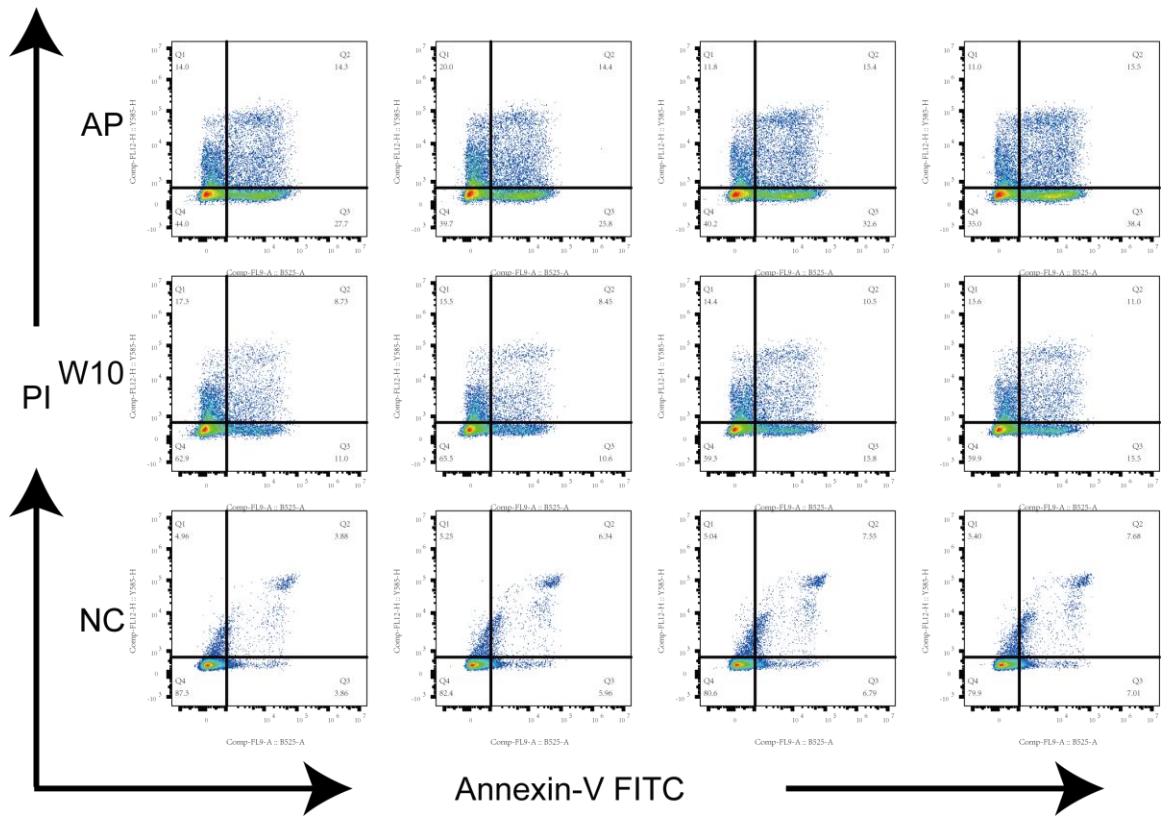


Figure S49. Flow cytometry analysis of COLO205 cell apoptosis following 48 h treatment with **AP** (10 μ M) and **W10** (10 μ M). Apoptosis detection by ANNEXIN V-FITC/PI double staining. NC, negative control.

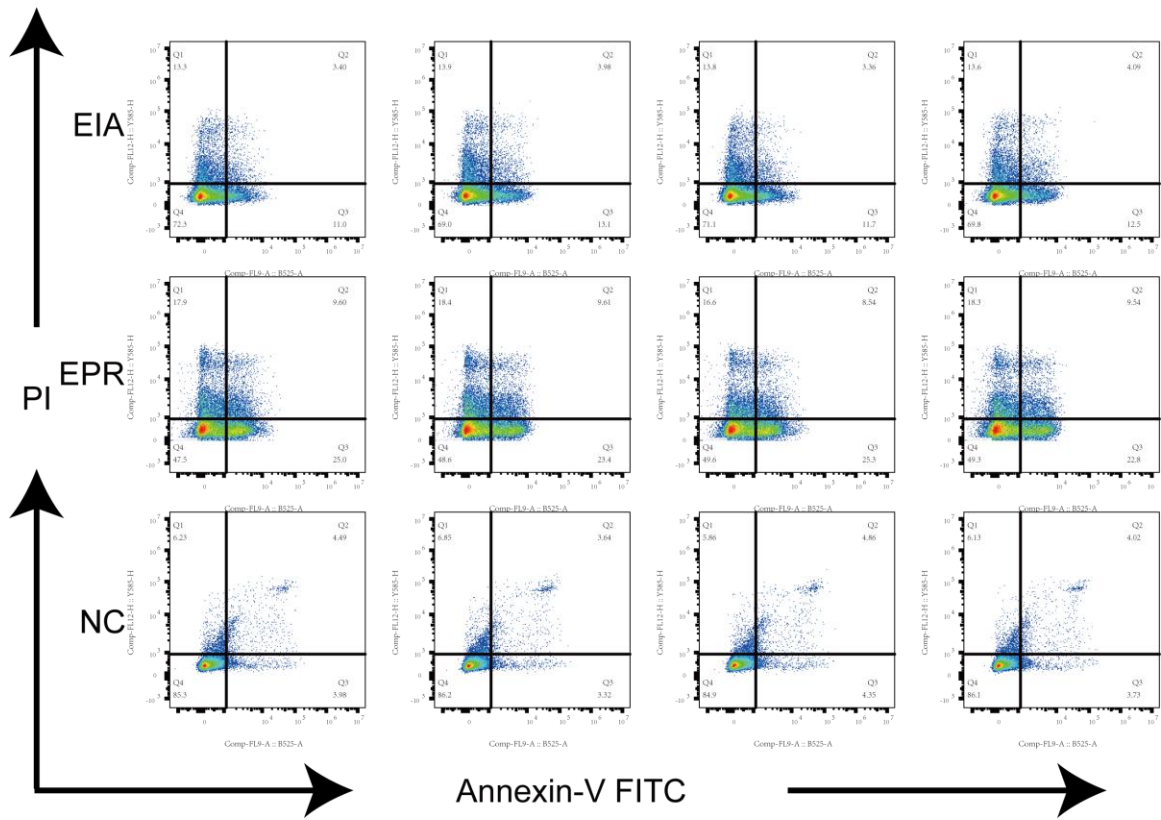


Figure S50. Flow cytometry analysis of COLO205 cell apoptosis following 48 h treatment with EIA (10 μ M) and EPR (10 μ M). Apoptosis detection by ANNEXIN V-FITC/PI double staining. NC, negative control.

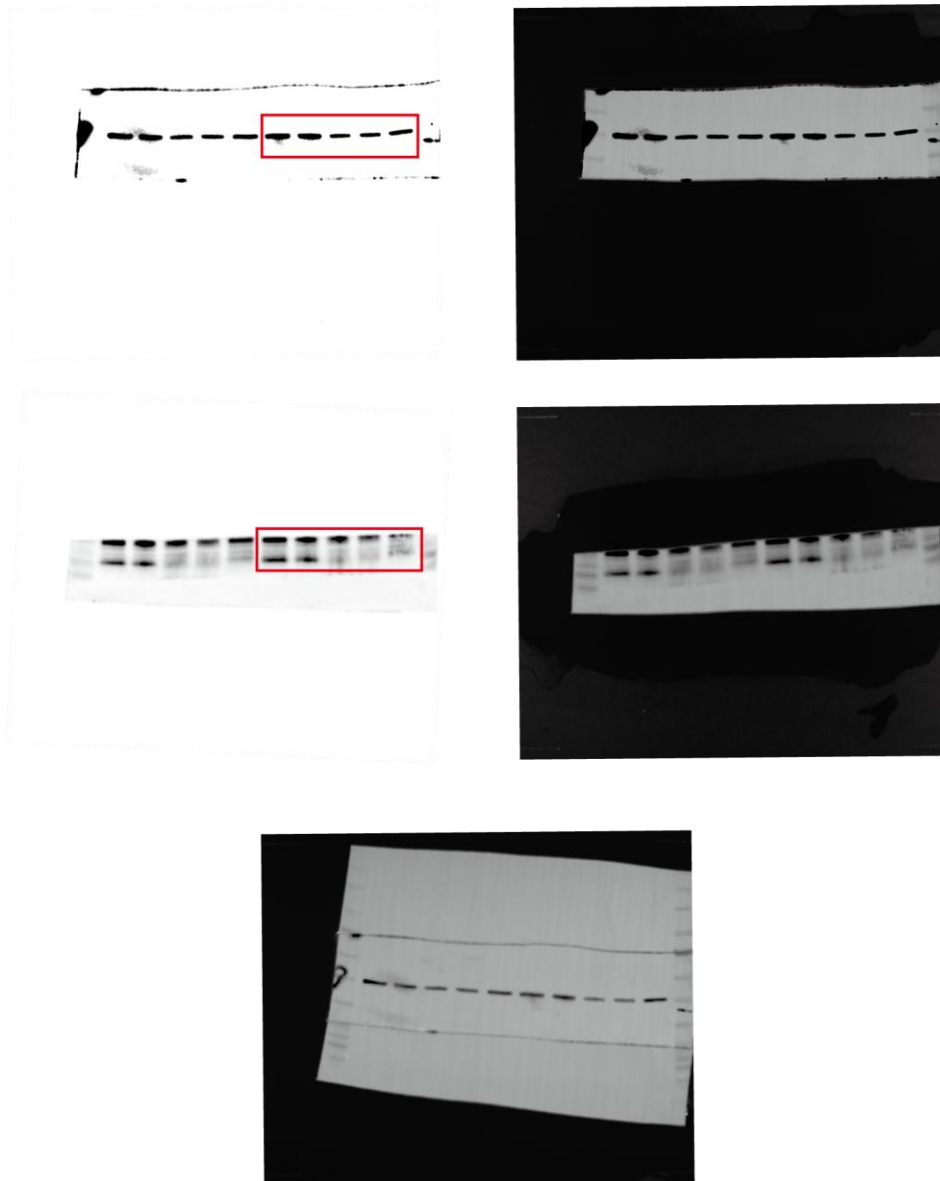


Figure S51. Unprocessed western blot images of cleaved caspase-3 and β -actin in COLO205 cells following AP and W10 treatment for 24 h and 48 h.

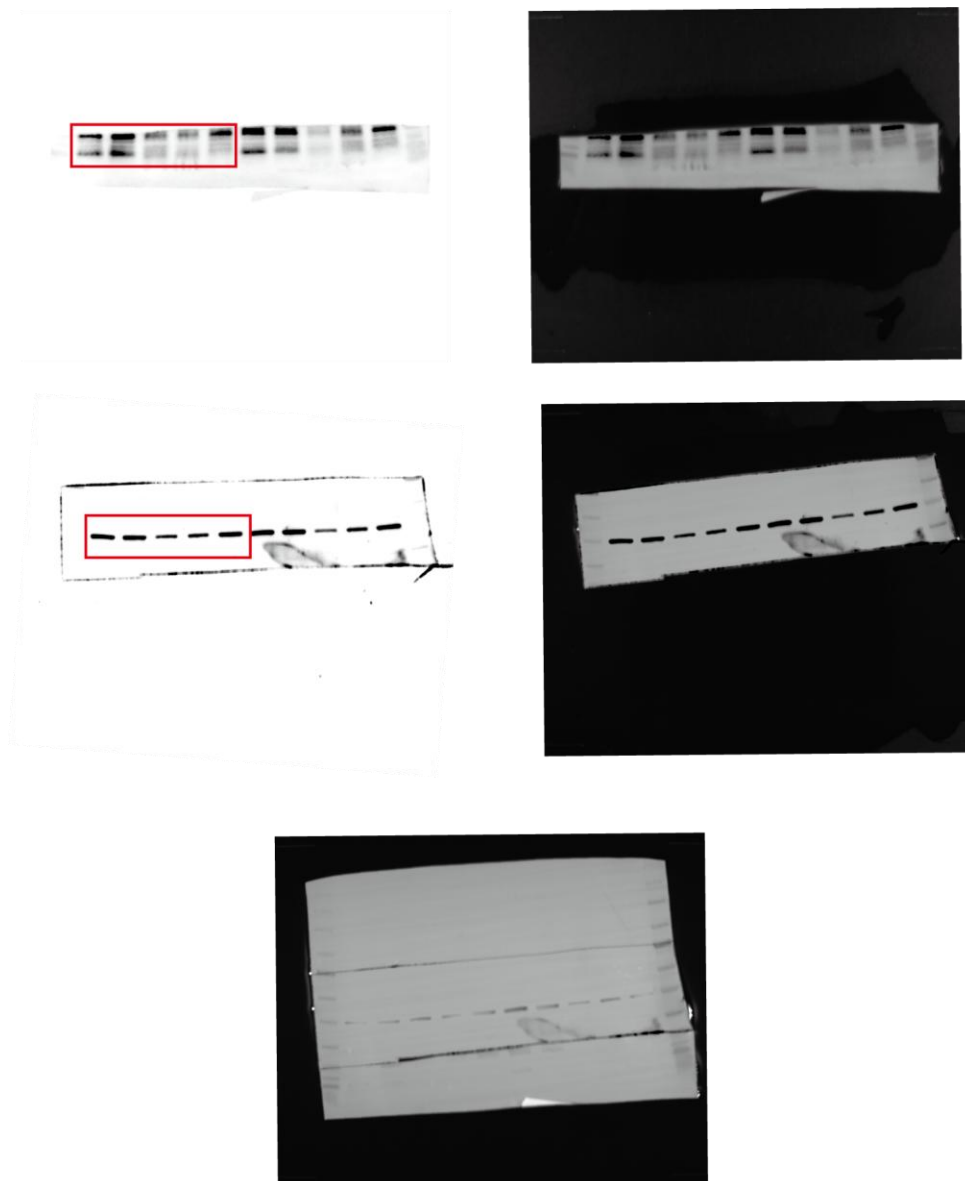


Figure S52. Unprocessed western blot images of cleaved caspase-3 and β -actin in COLO205 cells following EIA and EPR treatment for 24 h and 48 h.

Reference:

1. A. Micsonai, É. Moussong, F. Wien, E. Boros, H. Vadász, N. Murvai, Y.-H. Lee, T. Molnár, M. Réfrégiers, Y. Goto, Á. Tantos and J. Kardos, *Nucleic Acids Research*, 2022, **50**, W90 - W98.